

See discussions, stats, and author profiles for this publication at: <https://www.researchgate.net/publication/303080672>

Low-Cost and Low-Ringing Microstrip based Ultra-Wideband Pulse Generators using Step-Recovery Diode for Ground Penetrating Radar Applications

Thesis · August 2015

CITATIONS

2

READS

4,131

1 author:



Athar Kamal

Indian Institute of Technology Delhi

2 PUBLICATIONS 21 CITATIONS

SEE PROFILE

Some of the authors of this publication are also working on these related projects:



Project Feasibility study of Microwave imaging for planetary missions. [View project](#)

Low-Cost and Low-Ringing Microstrip based Ultra-Wideband Pulse Generators using Step-Recovery Diode for Ground Penetrating Radar Applications

Athar Kamal

**Low-Cost and Low-Ringing Microstrip based Ultra-Wideband
Pulse Generators using Step-Recovery Diode for Ground
Penetrating Radar Applications**

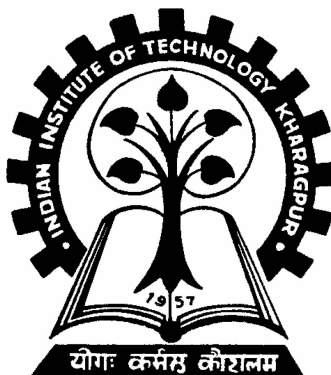
*Thesis submitted to the
Indian Institute of Technology, Kharagpur
For award of the degree
of
Master of Science(Research)*

by

Athar Kamal

Under the guidance of

Amitabha Bhattacharya



**Department of Electronics and Electrical Communication
Engineering**

Indian Institute of Technology Kharagpur

June 2014

©2014 Athar Kamal. All rights reserved.

This work is dedicated to my Parents, my Brother and my Fiance for their Constant
Support and Sacrifice.

Approval of the Viva-Voce Board

Date:

Certified that the thesis entitled **Low-Cost and Low-Ringing Microstrip based Ultra-Wideband Pulse Generators using Step-Recovery Diode for Ground Penetrating Radar Applications** submitted by **Athar Kamal** to the Indian Institute of Technology, Kharagpur, for the award of the degree of Master of Science (Research) has been accepted by the external examiners and that the student has successfully defended the thesis in the viva-voce examination held today.

(Member of the DSC)

(Member of the DSC)

(Member of the DSC)

(Supervisor)

(External Examiner)

(Chairman)

Certificate

This is to certify that the thesis entitled, **Low-Cost and Low-Ringing Microstrip based Ultra-Wideband Pulse Generators using Step-Recovery Diode for Ground Penetrating Radar Applications** submitted by **Athar Kamal** to Indian Institute of Technology, Kharagpur, is a record of bona fide research work under my supervision and I consider it worthy of consideration for the award of the degree of Master of Science (Research) of the Institute.

Signature of the Supervisor :

Prof. Amitabha Bhattacharya,

Associate Professor,

Electronics & Electrical Communication Engineering

Date:

Kharagpur

DECLARATION

I certify that

- (a) The work contained in the thesis is original and has been done by myself under the general supervision of my supervisor(s).
- (b) The work has not been submitted to any other Institute for any degree or diploma.
- (c) I have followed the guidelines provided by the Institute in writing the thesis.
- (d) I have conformed to the norms and guidelines given in the Ethical Code of Conduct of the Institute.
- (e) Whenever I have used materials (data, theoretical analysis, and text) from other sources, I have given due credit to them by citing them in the text of the thesis and giving their details in the references.
- (f) Whenever I have quoted written materials from other sources, I have put them under quotation marks and given due credit to the sources by citing them and giving required details in the references.

(Signature of the Student)

Curriculum Vitae

Athar Kamal was born in a village named Raj Gram in outskirts of West Bengal state, India, on May 26, 1987. He received the B.Tech degree in Electronics & Communication Engineering from the Netaji Subhash Engineering College (N.S.E.C.), affiliated to West Bengal University of Technology, West Bengal in 2010 and is currently working towards the Master of Science (Research) degree in RF & Microwave Engineering at the IIT Kharagpur. His research interests include RF & Microwave Integrated Circuits for Ultra Wideband Communication and Computational Electromagnetics. His publication is:

List of International Journal Publications

1. A. Kamal, A. Bhattacharya, M. Tamrakar and C. Roy, "Low-Ringing and Reduced-Cost Step Recovery Diode Based UWB Pulse Generators for GPR Applications," *Microwave and Optical Technology Letters.* (Accepted on 28th May, 2014)

Acknowledgment

First and foremost I thank The Almighty for the innumerable blessings and the testing situations which helped me throughout my life. I thank my parents, my brother and my fiancé for all the support, love, sacrifice and encouragement throughout this work. I would like to record my sincere gratitude to Prof. Amitabha Bhattacharya, my thesis advisor, for providing me this exciting research opportunity to work under his supervision in the area, which I like. His constant motivation, expert guidance and timely support, helped me at times to keep going on with enthusiasm and dedication towards the fulfillment of the work and to succeed in meeting very challenging deadlines, accomplishing much more in little time. He is an excellent mentor and I have learned a lot from him. I also thank The Indian Space and Research Organization for their faith that they showed by handing over the project which I worked on.

I thank all my DSC members for their support and suggestions throughout this work. I am so grateful to my senior and my lab-mate Mr. Nagavel Balasubramanyam. He has always been available for discussions related to my work and his contributions in this thesis are immeasurable.

Many thanks to Mr. Dhiraj Kr. Singh of LRDE, Bangalore who helped me kick start my research work. I am also thankful to Mr. Maruti Tamrakar and Mr. Chayan Roy of HCL Technologies Ltd., Chennai for fabricating the circuits and giving valuable suggestions regarding this work. I also thank Mr. Vishwanath, Mr. Sanjib Aditya and Mr. Pranab Kar for their support. I would like to thank Mr. Anindya Ghosh, Mr. Amit Srivastava, Mr. Rakesh Sinha, Mr. Moinul Haque, Mr. Tamesh Halder, Mr. Satyabrata Sarangi, Mr. Zishan Ali and all my friends at IIT Kharagpur, for their support, helping nature and making my stay memorable.

Date:

Athar Kamal

Kharagpur

Abstract

A low-cost pulse generator for Gaussian pulse and monocycle pulse generation using Step Recovery diode in series has been designed, implemented and tested. The circuit uses an attenuator for the purpose of reducing reflections that may distort the desired pulse shape at the output. It also provides a fair amount of impedance matching. The Step Recovery diode's characteristic of fast transition from low-impedance state to high-impedance state has been exploited and a Schottky diode has been employed to remove the unwanted ringing tail of the generated pulses. The circuit reliability is assured by the low jitter witnessed in the output waveforms. The fabricated circuit generates an $870mV$ Gaussian pulse having pulselwidth of $170ps$ between half maximum points. An added differentiator network shapes the Gaussian pulse into a monocycle pulse with $600mV$ peak to peak having $500ps$ duration between zero crossings. The generated monocycle pulse is having a fractional bandwidth of 162% . The measured waveforms were in good agreement with the simulated ones. Low cost and ultra-wideband performance is attributed to the use of a resistive attenuator and a single Step recovery diode. The low peak-repetition frequency and narrow pulselwidth facilitates deeper penetration for Ground Penetrating Radar by providing ample time for data sampling, storage and analysis.

Keywords: Attenuator, Ground penetrating radar, pulse generator, Pulsed power amplifier, pulselwidth, ringing, Step recovery diode, symbolically defined device.

Contents

Abstract	xiii
Contents	xv
List of Abbreviations	xvii
List of Symbols	xix
List of Figures	xxiii
List of Tables	xxv
1 Introduction	1
1.1 Motivation	2
1.2 A Review of Literature	2
1.2.1 Step Recovery Diode and its applications	2
1.2.2 Pulse generators	6
1.3 Problem Statement	7
1.4 Research Methodology	7
1.5 Organization of the Thesis	8
2 Overview of UWB Pulses	9
2.1 FCC regulations on UWB	10
2.2 Classification of UWB pulses and their properties	11
2.2.1 Orthogonality of UWB pulses	11
2.2.2 Orthogonal Gaussian pulses (OGP)	12
2.2.3 Orthogonal Modified Hermite pulses (OMHP)	13
2.2.4 Prolate Spheroidal pulses (PSP)	13
2.2.5 Inter-class Correlation	14

3 Step Recovery Diode Modeling	15
3.1 Step Recovery	16
3.2 The Minority Carrier Lifetime	18
3.3 Modeling of SRD	18
3.4 Analysis of SRD Model	22
4 Circuit Design and Simulation	25
4.1 Pulse Generation Concept	26
4.2 Design Description	27
4.2.1 Gaussian Pulse Generator Circuit	28
4.2.2 Monocycle Pulse Generator Circuit	35
4.2.3 Frequency Domain Analysis	38
5 Fabrication and Measurement	43
5.1 Fabrication	44
5.2 Measurement Results	45
5.3 Reliability Analysis	47
5.4 Relative Performance Evaluation	50
6 Suitability to GPR	53
7 Conclusion and Scope for Future Work	57
7.1 Conclusions	58
7.2 Scope for Future Work	59
A Matlab Codes for UWB waveforms	61
A.1 Family of Gaussian pulse	61
A.1.1 Basic Gaussian pulse	61
A.1.2 Monocycle pulse	62
A.1.3 Mexican Hat pulse	62
A.2 Orthogonal Modified Hermite pulse family	63
A.2.1 Zeroth order OMHP	63
A.2.2 First Order OMHP	63
A.2.3 Second Order OMHP	64
A.3 Prolate Spheroidal pulse family	64
B Plots of UWB waveforms	67
References	75

List of Abbreviations

ADS 2009 Advanced Design System 2009.

CAD Computer Aided Design.

CPW Co-planar Waveguide.

CSD Charge Storage Diode.

DHSRD Double Heterojunction Step Recovery Diode.

DSRD Drift Step Recovery Diode.

FCC Federal Communications Commission.

FWHM Full-Width-at-Half-Maximum.

GPR Ground Penetrating Radar.

MCL Minority Carrier Lifetime.

MMIC Monolithic Microwave Integrated Circuit.

OGP Orthogonal Gaussian Pulse.

OMHP Orthogonal Modified Hermite Pulse.

PPA Pulsed-Power Amplifier.

PRF peak repetition frequency.

PSD Power Spectral Density.

PSP Prolate Spheroidal Pulse.

RTD Resonant Tunnel Diode.

SD Schottky Diode.

SDD Symbolically Defined Device.

SRD Step Recovery Diode.

UWB ultra wide band.

List of Symbols

C_f Forward capacitance of SRD.

C_j junction capacitance of SRD.

C_r Reverse capacitance of SRD.

C_{dr} Total capacitance of diode in reverse bias.

C_{pk} Package capacitance of SRD.

D Ambipolar Diffusion constant.

D_n Diffusion constant for electrons.

D_p Diffusion constant for holes.

I_F Forward current or Charge injection rate into SRD.

I_R Reverse current or Charge withdrawal rate from SRD.

L_{TL} length of reverse transmission line.

L_{pk} Package inductance of SRD.

Q Charge stored at the junction.

Q_0 Stored charge from forward current after T_F .

R_S Series resistance in SRD model.

R_f Forward junction resistance of SRD.

R_x Shunt resistance of 3-dB attenuator network.

R_z Series resistance of 3-dB attenuator network.

R_{eq} Equivalent resistance of parallel combination of source and load resistance.

T Pulse duration of a Prolate Spheroidal pulse.

T_F Duration of injection.

T_P Pulse duration.

T_S Storage time of charges in SRD.

T_d delay introduced by shorted stub.

T_t Transition time of SRD.

T_{FWHM} FWHM of a temporal pulse.

V^+ Forward moving voltage wave.

V^- Reflected voltage wave.

V_b minimum breakdown voltage of SRD.

V_d SRD terminal voltage.

V_j Built-in potential of SRD.

Z_0 Characteristic impedance of transmission line.

Z_L Load impedance.

Z_S Source impedance of transmission line.

Δ_r Range resolution of a GPR device.

Δr_{min} Best range resolution of a GPR device.

Γ Reflection coefficient.

ϵ_0 Absolute permittivity of vacuum.

ϵ_e effective relative dielectric constant of substrate.

ϵ_r Relative dielectric constant of medium.

η Fractional bandwidth of signal.

η_{min} Minimum fractional bandwidth of a signal to be qualified as UWB.

λ Energy concentration of a pulse.

- μ Mean value for a Gaussian distribution.
- $\psi(t)$ Prolate Spheroidal pulse.
- σ Standard deviation for a Gaussian distribution.
- τ Minority carrier lifetime of SRD.
- c Speed of electromagnetic waves in vacuum.
- d dielectric height of microstrip substrate.
- d_0 Distance of center of mass of stored charges from junction.
- f_L Lower 10-dB frequency point.
- f_U Upper 10-dB frequency point.
- $g(t)$ Orthogonal Gaussian function.
- $h_n(t)$ Orthogonalized form of function $f_n(t)$.
- $h_{pn}(t)$ Hermite polynomial in t.
- $h_{pon}(t)$ Orthogonal modified Hermite polynomial.
- $m(t)$ First derivative of Gaussian function or Monocycle.
- $m_h(t)$ Second derivative of Gaussian function or Mexican hat pulse.
- t_{crt} Generator circuit's transition time (without SRD).
- t_{grt} Generator circuit's transition time.
- v electromagnetic wave velocity in sub-surface medium.
- v_P speed of electromagnetic wave along transmission line.
- w_m width of microstrip transmission line.
- $w(t)$ Weight function for orthogonalization.

List of Figures

2.1	FCC's PSD mask	10
3.1	CSD's I-V characteristics	16
3.2	Ceramic Epoxy Package	19
3.3	Small signal equivalent circuit of SRD in forward and reverse bias respectively.	20
3.4	SRD model employed in ADS Simulation	21
3.5	Model testing circuit	22
3.6	Output voltage waveform for a square wave input	22
3.7	Output voltage waveform for a sine wave input	23
4.1	SRD Pulse Generation Concept	26
4.2	Step waves' combination to the right of point A	27
4.3	Gaussian pulse generator circuit	28
4.4	Input Matching Circuit	29
4.5	Pulse generator output with no input matching circuit	29
4.6	Voltage across SRD	30
4.7	Conventional resistive symmetric π -network	30
4.8	(a) The implemented attenuator (b) Frequency response	32
4.9	Gaussian pulse generator output without attenuator	32
4.10	(a) Incident step and reflected step (b) Showing equality of Delay and FWHM	33
4.11	Gaussian pulse generator output without the rectifier	34
4.12	Output with source matched and attenuator and rectifier in place	34
4.13	Spectrum of the simulated Gaussian pulse	35
4.14	(a) Differentiator network (b) Frequency response of the differentiator	36
4.15	Monocycle Pulse generator circuit	37
4.16	Monocycle output	37
4.17	Spectrum of the Monocycle pulse	38
4.18	Spectrum of the step signal generated by SRD	39
4.19	Frequency response of the network without attenuator	39

4.20	Spectrum of the signal obtained without attenuator	40
4.21	Frequency response of the Gaussian pulse shaping section	40
4.22	Phase of transfer characteristics	41
4.23	Simulated circuit's S_{21} and group delay	41
5.1	Layout of the circuits	44
5.2	Photograph of fabricated circuits	44
5.3	The 10MHz source signal	45
5.4	(a) The generated Gaussian pulse and (b) its Spectrum	45
5.5	(a) The generated monocycle and (b) its Spectrum	46
5.6	Generated Gaussian Pulse plotted in MATLAB 2012B	46
5.7	Generated Monocycle plotted in MATLAB 2012B	46
5.8	Jitter analysis in the (a) Gaussian (b) monocycle pulse generator circuits	47
5.9	Comparison between simulated and measured Gaussian pulse	49
5.10	Comparison between simulated and measured Monocycle	49
6.1	A typical GPR configuration	54
6.2	Resolution comparison of different reported works for Gaussian pulse .	55
6.3	Resolution comparison of different reported works for Monocycle . .	55
B.1	Gaussian pulse (time domain)	67
B.2	Spectrum of the Gaussian pulse	68
B.3	Monocycle pulse (time domain)	68
B.4	Spectrum of the monocycle pulse	69
B.5	Mexican Hat pulse (time domain)	69
B.6	Spectrum of the Mexican Hat Pulse	70
B.7	OMHP 0 th order signal	70
B.8	Spectrum of OMHP 0 th order signal	71
B.9	OMHP 1 st order signal	71
B.10	Spectrum of OMHP 1 st order signal	72
B.11	OMHP 2 nd order signal	72
B.12	Spectrum of OMHP 2 nd order signal	73
B.13	APSP Signal	73
B.14	Spectrum of APSP signal	74

List of Tables

3.1	Dimensions in Inches [mm] of CS19-1 Package Style	19
3.2	Absolute Maximum Ratings of SRD (MSD-700)	19
3.3	Parameter Values of Modeled SRD	21
4.1	Specifications of RO4350B Laminate	28
4.2	Properties of the Simulated Gaussian Pulse	35
4.3	Properties of the Simulated Monocycle Pulse	38
5.1	Comparison between the Simulated and Measured Results	48
5.2	Comparison between Various Pulse Generators in Literature	50
5.3	Picosecond Pulse Labs Pulse generators [90]	51

Chapter 1

Introduction

Preface

This chapter deals with the introduction of the thesis. It comprises of an introduction in brief, literature review of Step Recovery Diodes (SRDs) and their applications and Pulse generators. It also gives the organization of the thesis.

1.1 Motivation

In our day to day life, we come across a lot of electronic devices and instruments which are constantly radiating fields of electromagnetic energy. In fact, two of the sense organs of human beings use this electromagnetic energy to work, viz. Eyes and Skin. Electromagnetics as a subject has been growing and is still under tremendous research. It has found its true worth in medical field, military, communication, geology and many domestic and research applications. Within this ever growing list, research fields like, Sedimentology, Glaciology, Hydrogeology etc. rely on Ground Penetrating Radars (GPRs). The heart of a GPR device is a Pulse Generator Circuit which has been a subject of constant research since the mid of 20th century. Currently, increasingly stringent requirements for pulse generators are narrower pulselwidth, lower ringing and higher power pulse generator circuits at lower cost. Now, for a good amount of penetration the power in the desired frequency band needs to be amplified. As a result, the input to the amplifier should be a well behaved pulse shape because amplification is not a very fidel operation.

1.2 A Review of Literature

1.2.1 Step Recovery Diode and its applications

During the mid of 20th century, research was going on to design circuits for efficient harmonic generation and fast switching circuits to work as good rectifiers. The varactors were used to design frequency doubler and tripler units and higher order multiplication used to be done by cascading these units. This cascading technique faced the problem of nonlinear interaction amongst them. The fast switching circuits used abrupt junction diodes. These diodes [1] had large storage phase and decay phase on the order of Minority Carrier Lifetime (MCL). They faced the problem of high residual charge which limited the rectification efficiency. A possible solution suggested in [1] was to increase the ratio of reverse to forward current. Works like [2] were going on to study the transient response of $p - n$ junction diodes having step graded impurity profile.

It was during early 1959 that while generating higher order harmonics, A. F. Boff discovered the step recovery effect. The step recovery effect was then witnessed and used for harmonic generation [3] in linearly and exponentially graded $p - n$ junctions. The latter showed a better transition time for a particular breakdown voltage. This class of diodes was introduced to the market in 1961 by Hewlett Packard. In order to gain insight on the charge storage and removal phenomenon, $p - n$ junction diodes' charge storing capability was investigated [4] and the various factors that affect the MCL were stated and explained. Stewart M. Krakauer named the class of diodes showing this effect of fast recovery as "Step Recovery Diode (SRD)" due to the abrupt variation of conductiv-

ity shown by them [5]. He also evaluated the rectification efficiency of such diodes and showed its dependence on circuit parameters, diode parameters including MCL. The research works on conventional varactors were also going on in parallel and the need of idler circuits was emphasized for generation of harmonics of order more than two [6]. The SRD also found its usage in generation of modulated signals [7] in communication schemes like Pulse Time modulation, Pulse Amplitude modulation and Frequency modulation. The SRD was then used to generate microwave power [8] using a single stage SRD multiplier. It proved to be less efficient than a varactors multiplier but, had the benefit of employing linear loads and generation of prime numbered harmonics. The first modeling work [9] to get an SRD model for the purpose of simulations had piecewise linear approximation of junction capacitance and junction resistance. In 1965, power was generated in L-band and X-band using resonant sub-circuit in the last stage of an SRD based frequency multiplier circuit [10]. The nonlinear characteristics of SRD were studied and a refined model [11] of SRD was given neglecting the residual charges. The varactors and SRDs were compared and it was found that the nonlinear junction resistance in SRDs made it look different than the conventional varactors. Some disheartening effects like hysteresis in a waveguide based millimeter wave generator [12] and additive phase noise generation [13] were witnessed. The phase noise minimizing technique by minimization of direct current through the diode was suggested. Another frequency multiplier circuit [14] was reported which used the SRD in shunt mode and a better-than-in-series isolation between input and output sub-circuit was obtained. The need of a proper circuit design [15] to ensure minimal distortion in the generated signal due to the SRD's nonlinear impedance was emphasized.

In the late 60s, the phenomenon of reverse recovery was theoretically established [16] and the need of a series inductance in the SRD model was explained [17]. Circuit design with the idler sub-circuit removed in a shunt mode SRD multiplier was theoretically and experimentally investigated [18], but instabilities or hysteresis could not be predicted. Harmonic generation works were reported on shunt mode SRD and the optimum terminating conditions [19] were estimated. A theoretical analysis of SRD based multipliers was performed which specified conditions to allow single conduction per input signal cycle [20], [21]. A general and explicit formula was given for power conversion efficiency variation with harmonic number [22] for SRD in series mode and a single efficiency estimation parameter [23] was also reported. Further modifications in the SRD CAD model were done to include the effect of nonzero transition time [24]. It was also illustrated that the width of $i - layer$ in a $p - i - n$ diode and the doping level had consequences on switching speed and diode losses [25]. The diode under consideration was an abrupt $p - i - n$ diode for which the ramping effect, fast transition and turn-off transient were discussed for the first time. It was inferred that the ramping and rounding-off effect could be minimized by making the doping profile more abrupt. During the 70s, asymmetric $p - n$ junction diodes were studied [26] and MCL down to

less than 1ns was measured. Numerical expression for MCL of abrupt doping profile junctions was formulated and a theory for minority carrier traps was proposed. These traps could decrease the storage time T_S or increase the transition time by increasing the residual charges. As reported, the dependence of ratio of MCL and T_S on ratio of forward current and reverse current was weakened by the recombination inhomogeneity [27] and impurity grading [26] and the two effects were shown to have a tendency to decrease the penetration length of the injected carriers. The reduction in MCL was reported [28] in an environment with intense neutron radiations like in a reactor or with gamma radiation, and it was shown that the circuit design parameters needed optimization for proper operation of the multiplier in such an environment. A minimum value of MCL was evaluated below which the recombination current will shoot up and result in efficiency degradation of the multiplier circuit. In an attempt [29] to reduce the pulse duration with minimal circuit elements, pulses in picosecond range were generated using two similar SRDs. The peak repetition frequency (PRF) was varied [30] from 1MHz to 40MHz and 10% variation was witnessed in pulse duration which ensured the circuit's reliable operation in timing circuits and ADC applications. Multiplier circuit [31] with high conversion efficiency was designed by driving the SRD from reverse conduction to Avalanche breakdown but it faced a major drawback of high dc power dissipation compared to the SRD being driven into cutoff. The first electronically tunable pulse generator [32] was designed which employed six SRDs in shunt mode to give a pulse train of 890ps duration with the intention of using it as a fast word generator, FM signal generator or an RF pulse generator. Pulse generators [33], [34] employing two SRDs in shunt were designed and tested to have risetime less than 100ps and duration from 150ps to 20ns, using Avalanche transistor as pulse signal source. A major drawback of pulse generator circuits employing SRD in shunt mode was highlighted here as the appearance of a slow ramp before the fast transition due to the SRD inductance. The course of SRD design faced a turn when asymmetrical $p - i - n$ diodes were investigated [35] and it was concluded that a reduction in doping of any of the two highly doped regions would result in a faster reverse recovery. A step further was taken in the SRD modeling work [36] by giving attention to the charges stored in the contact layers due to high injection. This modeling work assumed a thin $i - layer$ and a small diode area and gave an explanation for the rounding-off phenomenon observed for high charge injection.

In the 80s, pulse generator circuit design [37] was tested for sensing radars when signal was propagated in X-band. An error of 2% in distance measurement was recorded for metal and limestone targets. However, the circuit faced serious drawbacks of intense power loss. As the need of high power pulses for radar and spacecraft applications was increasing, it necessitated testing of the SRDs for their burnout threshold. It was inferred [38] that circuits generating pulses of lower duration were having a relatively higher failure pulser power. The research work in 90s witnessed a shift in the

design needs towards faster diodes and higher power generation. Double Heterojunction Step Recovery Diode (DHSRD) was investigated [39] for the first time and was successfully tested to have an astonishing transition time of 12ps. It was designed as $Al_{0.3}Ga_{0.7}As/Al_xGa_{1-x}As/Al_{0.3}Ga_{0.7}As$ and the mole fraction (x) was varied linearly from 0 to 0.15. This grading confined the carriers to the exit point and provided a drift field to hasten the charge removal process. High power $p - i - n$ diodes were canvassed [40] and reverse recovery was made faster by switching the diode off at the start of turn-on phase. The simplest model of SRD was molded [41] specifically for low injection case in step junction SRDs. The model was approximated with a current generator in parallel with a depletion capacitance. A further decrease in doping of $i - layer$ resulted in high mobility and high drift velocity [42]. These diodes showing high drift velocity were entitled as the Drift Step Recovery Diodes (DSRDs). The low doping of $i - layer$ facilitated high breakdown voltage and generation of high power microwave. SRD based frequency multiplier [43] was designed for the purpose of simulations such that it would consume lesser computing resources. The CPU time was reduced drastically without much error due to the deliberate nonlinearity reduction in the designed model. The DSRD structure was analyzed [44] and compared with the $p - i - n$ diodes. Conditions on the current density at the p^+n^- and n^-n^+ were formulated to minimize the ramping in DSRDs. High power rectifier diodes were operated in step recovery mode to generate high power pulses having a peak voltage of 2kV and 0.7ns duration [45]. A repetition rate of 10kHz was tested and reliable performance was achieved, it was estimated that the repetition rate could be increased to 50kHz with appropriate cooling techniques.

With the start of the 21st century, technology became cheaper and reforms were made by the Federal Communications Commission (FCC) relaxing the restrictions [46] on Electromagnetic spectrum usage in domestic, commercial and research applications. The design of pulse generators in time-domain, gained popularity and low cost planar circuits employing SRDs [47]–[54] were reported, having monocyte generation capabilities. SRD modeling work was refined [53] to show a better nonlinear approximation of its behavior. Monolithic Microwave Integrated Circuits (MMICs) amplifier and MESFETs were employed to provide higher amplitude, better isolation and higher PRF. DSRD was used to generate 1.8kV pulses with 50kHz PRF, 64.8kW peak power, 100ps risetime and a very low jitter [55]. Pulse generator design using two shunt mode SRDs was reported [56] to have good Full-Width-at-Half-Maximum (FWHM) of the generated Gaussian pulse as 241ps and 5.6V peak but the pulses were not having a good symmetry in shape and ringing was high. A formidable work [57] on designing of ultra wide band (UWB) sampling receiver for impulse Ground Penetrating Radar (GPR) systems was reported. It had merits like smaller area, low cost, simple structure, higher efficiency, wide sampling bandwidth and better sensitivity. It was shown to have a detection depth of 48cm and resolution of 6mm as it could very well detect steel pipes of 6mm

diameter buried 48cm deep in sand. A cascade of SRDs was used with two in series and one in shunt to generate Gaussian pulses in picosecond range. The signal reported [58] in this work had a high ringing, probably due to the SRD used in shunt mode. SRDs in shunt mode necessitate the inclusion of inductance in the circuit for biasing purpose which makes the circuit bulkier and susceptible to radiations. The newborn concept of DSRD was further investigated [59] numerically to explain its switching mechanism. It was pointed out that narrowing of the base region (low doped p layer) could increase the peak voltage of pulses generated. Another pulse generator design [60] was worked out with low ringing (less than -22dB) in generated monocyte. The pulse generator was fed with a 10Vp-p square-wave input and it used an attenuator ($BW - N20W5+$ of Mini-circuits) to gain proper impedance match. The monocyte was highly attenuated but it had low ringing and short duration. A bipolar pulsed power circuit design [61] was reported to act as a test bench for DSRD characterization. A recently reported [62] pulse generator employed four Silicon power transistors in Avalanche mode, two SRDs and four Schottky Diodes (SDs) to generate high voltage positive and negative pulse output. SRDs with very high breakdown voltage were required in the pulse shaping circuit. Among the applications of an SRD based pulse generator, some can be enlisted as: pavement damage detection [63], cancer detection [64], indoor ranging [65], through-wall imaging [66], [67], buried landmine detection [68], rescue operations [69] and wireless impulse-power transfer and reception [70]. Pulse generator designs have also been reported to construct microwave sampler circuits [71], [72] aiming to replace the mixer, voltage controlled oscillator and the phase-lock loop from receiver module of millimeter-wave radars.

1.2.2 Pulse generators

The negative differential resistance characteristic of Tunnel diodes has been exploited for pulse generation where it behaves as a monostable switch. The pulse generator circuit [73] has been successfully tested for 2GHz PRF in high speed counter applications. Pulse generator [74] having capability to give pulses corresponding to leading or trailing edge of driving signal was reported. These diodes could produce very narrow pulses but amplitude of the pulses was low. The Resonant Tunnel Diodes (RTDs) evolved as high speed switching diodes for terahertz applications. They were used for fast pulse generation and with the use of tapered transmission lines, peak power output of the pulse was increased by 30% [75]. Transistors driven in Avalanche breakdown mode were also being used for high repetition rate pulse generation [76], [77]. High amplitude of 1.1kV with sub-nanosecond risetime was obtained for repetition rate of 200kHz [78]. Pulse generator circuit in CMOS technology was reported [79] to generate monocyte with 380ps duration and 660mV peak-peak voltage for cardio-pulmonary monitoring. The CMOS based pulse generators have a long development time and are cost-ineffective for low-volume production. Moreover, they have been used for low power applications

[80] and high PRF [81] ranges on the order of gigahertz which is suitable only for very low range detection applications. Transistors operated in Avalanche breakdown mode demand high caution as the issues like heat dissipation and probable non-linearity cannot be undermined while using this method for pulse generation. The Tunnel diodes and Avalanche transistors were outsmarted by the SRDs, mostly due to the limited lifetime of Avalanche transistor based pulse generators and the limitedness of maximum obtainable voltage by a Tunnel diode based pulse generators [82]. The most common method used for pulse generation has been by using SRD. The unique snap off characteristic of SRD has been used for pulse generation where the SRD has either been used in shunt mode or series mode. Many impulse radars belonging to the class ennobled Ground Penetrating Radar have been designed to detect, identify and characterize hidden objects and also the ones beneath the ground by transmitting and analyzing the received signal.

1.3 Problem Statement

Main objective of the research work is to fabricate an SRD based pulse generator. The pulses should have low ringing characteristics and the pulselwidth should be narrow enough to have a best resolution capability Δr_{min} of 3.75mm over dry sand $\epsilon_r = 4$ which corresponds to a pulselwidth of 100ps. It should be cost effective for GPR applications in UWB range and should be fabricated using microstrip technology.

1.4 Research Methodology

The objective can be segmented into the study, design, simulation, analysis and fabrication of the SRD based pulse generator. A general methodology for the design of the generator circuit has been followed focusing on the pulse shaping circuitry for a signal generated having good symmetry and low ringing. Then measurements will be done to extract dc parameters like threshold voltage and forward resistance. Due to the unavailability of an SRD model for simulation purpose, one has to be designed taking all the characteristic and parasitic parameters into consideration. Using the SRD model, a pulse generator circuit will be designed that meets our requirement of pulse and circuit characteristics. The source signal needs to be chosen taking the requirements into account. The substrate material or the laminate has to be chosen to be cost effective and should be usable within the frequency limits. The pulse generator circuit will be designed in the Agilent's Advanced Design System 2009 (ADS 2009) platform. After getting a convincing output signal, fabrication work will follow.

1.5 Organization of the Thesis

- Chapter 1

This chapter deals with the introduction of the thesis. It comprises of an introduction in brief, literature review of SRDs and their applications and Pulse generators. It also gives the organization of the thesis.

- Chapter 2

In this chapter an overview of the UWB pulses is given which is a study on the various prospective pulse shapes for UWB communication.

- Chapter 3

In this chapter the SRD has been discussed and its modeling work in ADS 2009 is presented. The model has also been analyzed using simulations. Design equations, figures and tables have also been included.

- Chapter 4

This chapter discusses the designing procedure and the design of a pulse generator. Each segment of the design has been separately discussed and analyzed. Design equations, figures, tables and simulation results have also been added.

- Chapter 5

In this chapter, the measurement results are presented and compared with the simulation results. Figures showing and comparing the results and tables are also included.

- Chapter 6

This chapter deals with the analysis of the aptness of the designed circuit for being used in GPR applications. Figures and tables are included to get a better understandability.

- Chapter 7

Finally, conclusions of the work carried out and suggested future scope of studies are given in this chapter.

Chapter 2

Overview of UWB Pulses

Preface

In this chapter an overview of the UWB pulses is given which is a study on the various prospective pulse shapes for UWB communication.

The FCC adopted changes in UWB regulation on February 14, 2002 as *FirstReportandOrder, ET Docket98-153* [46] and released it on April 22, 2002. It made the use of UWB license-free which enticed researchers and concerned industries across the globe to use it in any and every way for academic, business and research purpose.

The FCC also imposed a set of rules on spectral masks for maximum allowable transmission power for UWB applications. These spectral limitations (in order to avoid its potential interferences with existing communication systems) created challenges in signal generation and transmission of UWB system. This emphasizes the need of an in-depth study on UWB signal shapes.

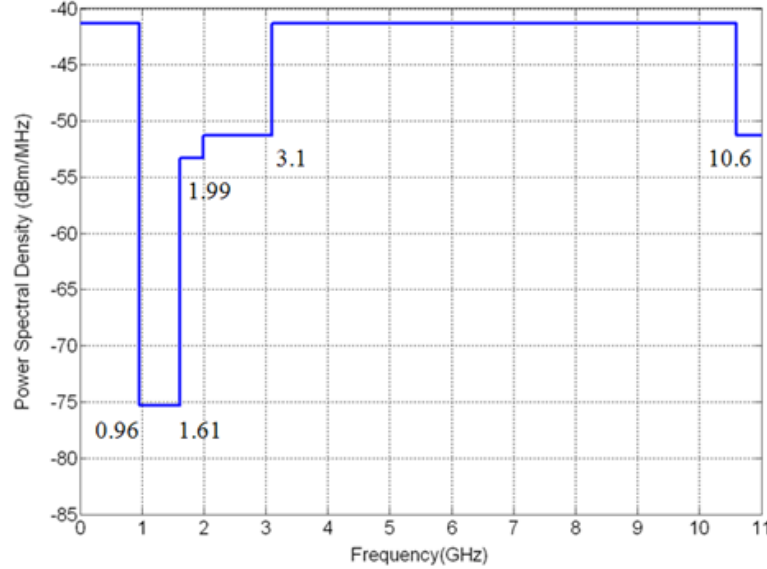


Figure 2.1: FCC's PSD mask

2.1 FCC regulations on UWB

Some of the restrictions imposed on signal characteristics for UWB can be stated as follows:

- (a) The minimum bandwidth measured at points 10dB below the peak power level is 500MHz for signals having greater than 2.5GHz center frequency else the fractional bandwidth (η) (2.1.1) obtained by taking the upper (f_U) and lower (f_L) frequency points, should be at least 0.20.

$$\text{Fractional Bandwidth} = 2 \left(\frac{f_u - f_l}{f_u + f_l} \right) = \frac{\text{Bandwidth}}{\text{Center Frequency}} \geq 0.20 \quad (2.1.1)$$

- (b) The permissible Power Spectral Density (PSD) for UWB signals in the band from 3.1 GHz to 10.6 GHz was set at -41.3 dBm/MHz .
- (c) GPS band being used for many critical operations for public safety, navigational purposes and spotting emergency locations had to be free of any interference probability.
- (d) GPR devices were allowed to operate in any part of the spectrum, provided the signal was shot vertically to the ground and the device had a turn-off switch with an operator.

The UWB spectrum usage limits are shown in Figure 2.1. It gives an idea about the shape of spectrum which the signals should have for being used in the license free UWB band.

2.2 Classification of UWB pulses and their properties

The term pulse has been rigorously used to emphasize the time-limitedness of the signal. The existing UWB pulses have been categorized [83] as Orthogonal Gaussian Pulse (OGP), Orthogonal Modified Hermite Pulse (OMHP) and Prolate Spheroidal Pulse (PSP). An introduction to the families of UWB pulses has been given with special emphasis on Gaussian pulse's family.

2.2.1 Orthogonality of UWB pulses

The UWB pulses are bound to have a wide bandwidth and as a result they will interfere with signals in other licensed communication channels like GPS. To prevent interference of UWB signal with those in licensed bands, the condition of Orthogonality of functions expressed in (2.2.1) is imposed on pulse shapes.

$$\int_{-\infty}^{\infty} f_n(t) * f_m(t) dt = 0; \quad n \neq m \quad (2.2.1)$$

The condition above is satisfied only by orthogonal functions. For non-orthogonal functions, a weight function $w(t)$ is used to make it orthogonal.

$$\int_{-\infty}^{\infty} f_n(t) * f_m(t) * w(t) dt = 0; \quad n \neq m \quad (2.2.2)$$

The weight function is included with the function $f_n(t)$ and expressed as $h_n(t)$ representing the orthogonalized function.

$$h_n(t) = \sqrt{w(t)} * f_n(t) \quad (2.2.3)$$

Now, the function $f_n(t)$ is orthogonalized and its orthogonality can be checked as,

$$\int_{-\infty}^{\infty} h_n(t) * h_m(t) dt = 0; \quad n \neq m \quad (2.2.4)$$

2.2.2 Orthogonal Gaussian pulses (OGP)

It represents a class of pulses that resemble the famous Gaussian function with σ and μ as parameters and is mathematically represented as (2.2.5).

$$g(t) = \frac{1}{\sigma\sqrt{2\pi}} e^{\left(\frac{1}{2}\left(\frac{t-\mu}{\sigma}\right)^2\right)} \quad (2.2.5)$$

This family of pulses comprises of the basic Gaussian pulse and its derivatives. The basic Gaussian pulse is defined for a pulse-duration T_P and normalized amplitude. Assuming,

$$\mu = \frac{T_P}{2}; \quad \sigma = \frac{T_P}{7} \quad (2.2.6)$$

The basic Gaussian pulse can be represented as

$$g(t) = e^{\left(\frac{1}{2}\left(\frac{t-\frac{T_P}{2}}{\frac{T_P}{7}}\right)^2\right)} \quad (2.2.7)$$

The factor is as a result of orthogonalization [83] of the Gaussian pulse. Derivatives of $g(t)$ or the filtered forms of $g(t)$ have higher center frequency and lower bandwidth. The first derivative is a monocycle ($m(t)$) and is represented by (2.2.8).

$$m(t) = -\frac{49}{T_P^2} * \left(t - \frac{T_P}{2}\right) * e^{\left(\frac{1}{2}\left(\frac{t-\frac{T_P}{2}}{\frac{T_P}{7}}\right)^2\right)} \quad (2.2.8)$$

The second derivative of $g(t)$ is a Mexican Hat pulse ($m_h(t)$) and is represented by (2.2.9).

$$m_h(t) = \left[\left(\frac{49}{T_P^2} \right) * \left\{ -1 + \frac{49}{T_P^2} \left(t - \frac{T_P}{2} \right)^2 \right\} \right] * e^{\left(\frac{1}{2}\left(\frac{t-\frac{T_P}{2}}{\frac{T_P}{7}}\right)^2\right)} \quad (2.2.9)$$

2.2.3 Orthogonal Modified Hermite pulses (OMHP)

The class of polynomials represented by (2.2.10) is called Hermite polynomials ($h_{pn}(t)$) [83].

$$h_{pn}(t) = (-T_P)^N * e^{\frac{t^2}{2T_P^2}} * \frac{d^n}{dt^n} \left(-e^{\frac{t^2}{2T_P^2}} \right) \quad (2.2.10)$$

These polynomials are orthogonalized and are represented as Orthogonal Modified Hermite polynomials ($h_{pon}(t)$) in (2.2.11)

$$h_{pon}(t) = (-T_P)^N * e^{\frac{t^2}{4T_P^2}} * \frac{d^n}{dt^n} \left(-e^{\frac{t^2}{2T_P^2}} \right) \quad (2.2.11)$$

The mathematical representation of UWB pulses belonging to this family can be obtained for different values of n .

2.2.4 Prolate Spheroidal pulses (PSP)

The mathematical representation of pulses in this family is obtained as solutions of a second order differential equation (2.2.12).

$$\frac{d}{dt} \left\{ (1-t^2) \frac{d\psi(t)}{dt} \right\} + (\lambda - c^2 t^2) \psi(t) = 0 \quad (2.2.12)$$

For different values of λ which represents the energy concentration of the pulse, different expressions for $\psi(t)$ are obtained.

$$\lambda = \frac{\int_{-\frac{T}{2}}^{\frac{T}{2}} |\psi(t)|^2 dt}{\int_{-\infty}^{\infty} |\psi(t)|^2 dt} \quad (2.2.13)$$

Solving the equation is a very difficult task and it only gives approximate solutions. In [84] an approximate solution was found and was represented as in (2.2.14) with T as its duration and c as the speed of an electromagnetic wave in vacuum.

$$\psi(t) \approx \frac{\sin \left[c \sqrt{\left(\frac{t}{T}\right)^2 - 1} \right]}{\sinh(c) \sqrt{\left(\frac{t}{T}\right)^2 - 1}} \quad (2.2.14)$$

2.2.5 Inter-class Correlation

The pulses belonging to the class of OGP are same as the OMHP except for an amplitude-scaling factor and a time-scaling factor. The PSPs are orthogonal in nature and hence their weight function is 1.

All these classes belong to solutions of the famous second-order differential equations representing different Sturm-Liouville boundary value problems. So, they cannot be time-limited theoretically, but the PSPs are considered within the time limit $[-T/2, T/2]$ and due to this time-limitedness the pulses belonging to PSP class are relatively more immune to jitter.

The other way of enforcing time-limitedness is to use fast decaying pulses. This can be achieved by differentiating the basic pulse and using the higher order derivatives. Both the OGP and OMHP class use derivatives to change the shape and increase spectral efficiency whereas the PSP uses variation of energy concentration in the pulses.

It has been shown [85] in literature that the odd-order derivatives of the basic Gaussian pulse are having a better spectral efficiency compared to the even-order derivatives. A comparison [86] based on auto-correlation function of UWB pulses was reported which stated that monocycle pulse is best among the possible pulses w.r.t. spectrum shape, precision for radar applications and realization complexity.

A Matlab code to generate the studied signals $g(t)$, $m(t)$, $m_h(t)$, $h_{pon}(t)$ (0^{th} , 1^{st} and 2^{nd} order), $\Psi(t)$ is included in Appendix A and the obtained plots are included in Appendix B.

Chapter 3

Step Recovery Diode Modeling

Preface

In this chapter the SRD has been discussed and its modeling work in Advanced Design System 2009, is presented. The model has also been analyzed in simulations. Design equations, figures and tables have also been included.

3.1 Step Recovery

A new class of p-n junction diodes emerged in late 1950s which had remarkable applications like harmonic generation, wave shaping and pulse generation. These diodes were reported to have the capability to store charges in the reverse conduction mode. They were entitled as Charge Storage Diodes (CSDs). The property of charge storage was mainly due to a large MCL. The charges are accumulated near the junction, as a result of injection in forward bias condition. During the forward bias, when an equilibrium is attained between the constant charge injection rate (I_F) and recombination rate, the bias changes to reverse mode and the injection stops. In reverse mode, the overall operation is termed as reverse recovery. The term reverse stands for the bias and recovery stands for the recovering of charges that had been injected but were not received at the diode's other terminal. So, the bias was changed to recover those charges. This reverse recovery phase comprises of storage phase, transition phase and decay phase. In the beginning of reverse recovery phase, the diode is in a reverse storage conduction mode (shown in Figure 3.1) when a constant reverse current (I_R) flows and the diode shows a small resistance as in forward conduction mode.

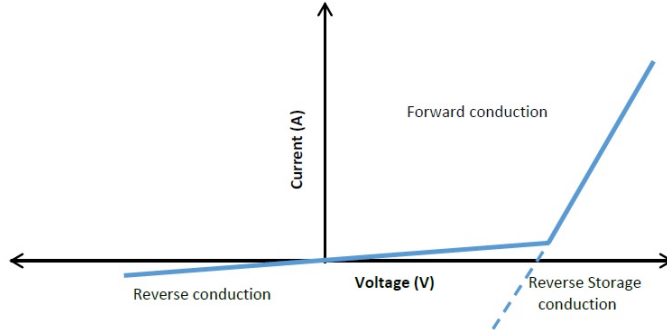


Figure 3.1: CSD's I-V characteristics

The duration of storage phase depends extensively on MCL (τ), doping profile of the junction and charge stored in forward bias mode. The charge continuity equation (3.1.1) is analyzed to obtain the amount of stored charge.

$$\frac{dQ}{dt} = I - \frac{Q}{\tau} \quad (3.1.1)$$

or, $Q_0 = I_F \tau \left(1 - e^{-\frac{T_F}{\tau}}\right)$

Assuming, $T_F \gg \tau$,

$$Q_0 = I_F \tau \quad (3.1.2)$$

Equilibrium needs to be attained between the injection and recombination of charges, so that steady state of charge stored is obtained. The total charge stored (Q_0) in the forward conduction mode is neutralized by recombination and removed by the reverse current. The duration of storage phase can be mathematically estimated using (3.1.3) [58].

$$T_S = \tau * \ln \left[1 - \frac{I_F}{I_R} \left(1 - e^{-\frac{t_F}{\tau}} \right) \right] \quad (3.1.3)$$

The second phase is the transition phase which is an abrupt change of diode impedance from a low value (few Ω s) as in forward conduction to a very high value (few $M\Omega$ s) corresponding to cutoff mode. The abruptness of this transition (3.1.4) depends on the separation of the stored charge's center of mass from junction (d_0) and the ambipolar diffusion constant (D) (depending on D_n and D_p) of the carriers injected (3.1.5).

$$T_t = \frac{d_0^2}{D} \quad (3.1.4)$$

$$D = \frac{2D_n D_p}{D_n + D_p} \quad (3.1.5)$$

The separation, d_0 can be reduced by using a diode with graded doping profile, which facilitates the growth of retarding field across the junction and restricts the minority carrier spreading, hence reducing d_0 .

Now, this abrupt transition of diode conductivity approximates a step jump entitling the phenomenon as step recovery. The sub-class of the diodes belonging to the class of CSDs, and showing such an abrupt transition is called the STEP RECOVERY DIODE. The third phase is the decay phase which is unwanted, as it introduces ringing in current through diode. The duration of this phase can be reduced if all the minority carriers are located close to the junction so that they can be removed efficiently by the reverse current leaving a negligible amount of residual charges. Now, if the amount of stored charge is high, the charge density will increase and hence the center of mass will be forced to shift away from the junction making their removal, less probable. For a step junction, the duration of decay phase is comparable to the MCL, whereas for a graded junction, it is several orders less.

An ideal SRD has the following characteristics.

- (a) An infinite forward capacitance (C_f) so that the terminal voltage does not change during forward conduction (3.1.6).

$$C_f = \frac{I_f}{dV_d/dt} \quad (3.1.6)$$

- (b) An infinitesimal transition time for transition from reverse storage conduction to

cutoff.

- (c) Reverse capacitance, C_r should be negligibly small (3.1.7) so that it can accommodate an infinite voltage transition rate, for harmonic generation application.

$$C_r = \frac{I_r}{dV_d/dt} \quad (3.1.7)$$

- (d) The MCL should be large, but its large value limits the peak repetition frequency of the input signal .
- (e) Parasitic elements are negligibly small. However, a small amount of series inductance is needed for harmonic generation applications.

The parasitic effects in an actual SRD which are basically the modeling approximations of the deviation from expected characteristics of the SRD due to diode package and discontinuity in the biasing and matching circuitry can be enlisted as:

- (a) The package capacitance (C_{pk}), package inductance (L_{pk}) and series resistance (R_s) make the diode under-damped, for modeling the rounding effect and ringing which are present in an actual SRD.
- (b) The series resistance should be as low as possible to minimize the diode losses and reduce the transition time by reducing the time constant of diode transition phase. The L_{pk} and R_s together approximate the ramping effect in SRD [33].

3.2 The Minority Carrier Lifetime

In earlier times, diodes were fabricated to have a low MCL, to avoid the reverse conduction which was unwanted as the diodes were mostly used as rectifiers and switches. After the invention of SRDs, there arose a need of higher MCL. For rectification and switching applications, the MCL should be low, so that the diode behaves as a voltage dependent resistor. However, for an SRD designed for harmonic generation, it should ideally be infinite, for the diode to act as a voltage dependent capacitor [5]. Its value depends on various parameters [4] like: diode area, impurity density profile, operating temperature, charging current and recombination trap density.

3.3 Modeling of SRD

Due to the unavailability of a working SRD simulink model, its modeling is of prior importance so that the circuit design simulations and analysis can be carried out for the

SRD based circuits. The SRD that we intend to use is MSD-700 of Aeroflex Metelics, packaged in Ceramic epoxy package. Dimensions of the package are shown in Figure 3.2 and the values are specified in Table 3.1. The SRD specifications are as shown in the Table 3.2.

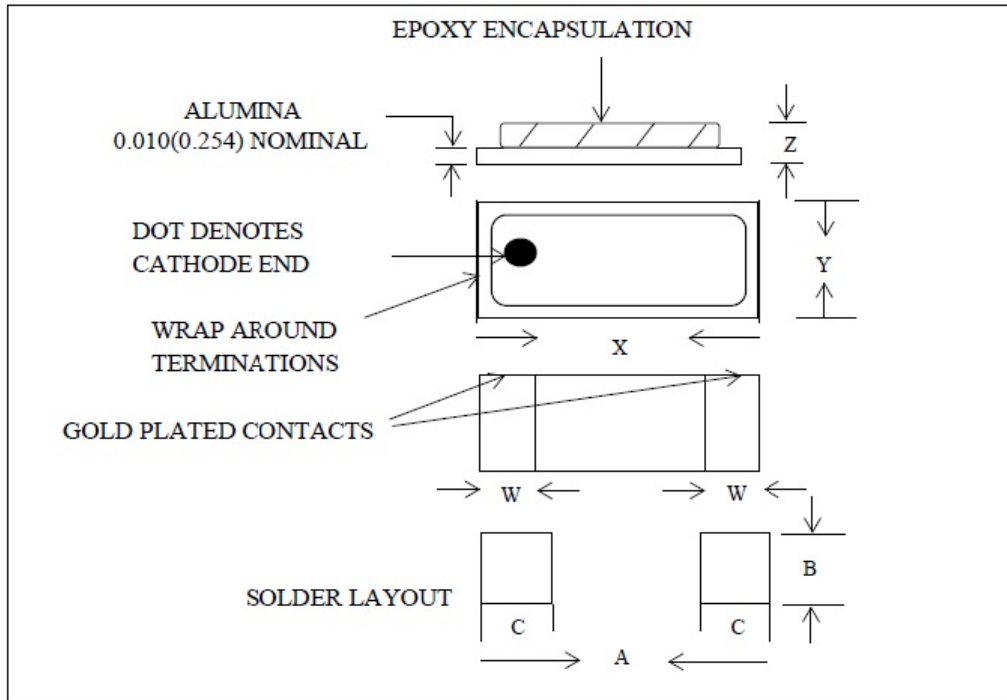


Figure 3.2: Ceramic Epoxy Package

Table 3.1: Dimensions in Inches [mm] of CS19-1 Package Style

Package Style	Dimensions				Solder Layout(Typical)			$C_{pk}L_{pk}$
	W	X	Y	Z	A	B	C	
CS19-1	0.012 [0.304]	0.060 [1.52]	0.040 [1.01]	0.030 [0.762]	0.072 [1.83]	0.040 [1.01]	0.020 [0.058]	0.09 0.35

Table 3.2: Absolute Maximum Ratings of SRD (MSD-700)

Junction Capacitance, C_j at -6V, 1MHz(pF)	Minimum Breakdown Voltage, V_b at $10\mu A$ (V)	Minimum Carrier Lifetime, τ_{min} at $I_r=6mA$, $I_f=10mA(ns)$	Max. Transition Time, T_t (ps)	Max. Series Resistance, R_S at $I_f = 25mA(\Omega)$
0.2 - 0.4	15	8	60	1.20

The SRD being a strongly nonlinear device, its modeling is undoubtedly a big challenge. Basically, SRD acts as a switch from the high impedance state to low impedance state corresponding to a small reverse bias capacitance and an infinite forward bias capacitance. However, for modeling purpose, we need to consider a finite C_r for the SRD. The modeling work of the SRD is done in Agilent's ADS 2009 simulation platform. Small signal equivalent circuit of the SRD is shown in Figure 3.3.

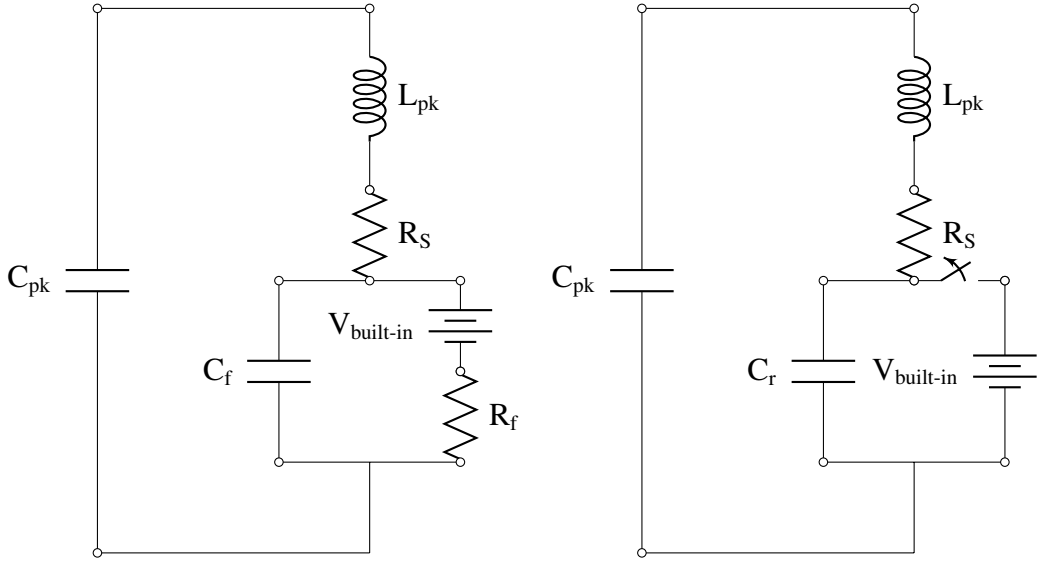


Figure 3.3: Small signal equivalent circuit of SRD in forward and reverse bias respectively.

The Symbolically Defined Device (SDD) was used to model the forward and reverse capacitance of the SRD. The modeling equation [43] which is used in this work by incorporating it in the SDD is shown in 3.3.1.

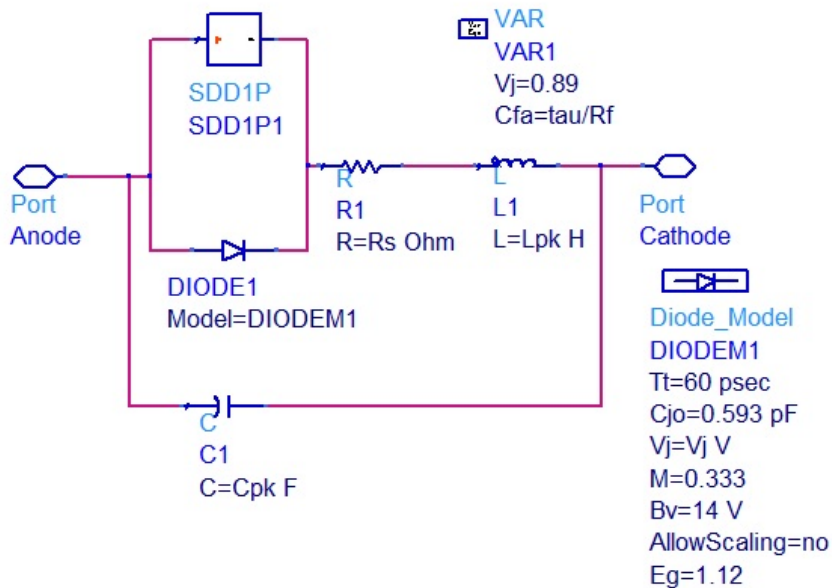
$$Q_{Vd} = \begin{cases} C_r * V_d & V_d \leq 0 \\ \frac{C_f - C_r}{2V_j} \left(V_d + \frac{C_r V_j}{C_f - C_r} \right)^2 - \frac{C_r^2}{2(C_f - C_r)} * V_j & 0 < V_d < V_j \\ C_f V_d - \frac{C_f - C_r}{2} V_j & V_d \geq V_j \end{cases} \quad (3.3.1)$$

In the above equation, Q stands for charge stored in the diode, V_d is the diode terminal voltage and V_j represents the built-in potential of the diode under consideration. C_r (0.3pF at a reverse bias of 6V, as specified by manufacturer) represents a very small but finite capacitance corresponding to the reverse bias state of the diode. C_f is the maximum value of the forward bias capacitance that depends on forward bias resistance R_f of the diode and the MCL (τ) according as (3.10).

The modeled SRD is shown in Figure 3.4 whereas the parametric values that were used in the modeling are specified in Table 3.3.

Table 3.3: Parameter Values of Modeled SRD

Parameter	Values
MCL (τ)	8ns
Transition Time T_t	60ps
Built-in Potential V_b	0.890V
Forward junction resistance R_f	1.040Ω
Capacitance at zero bias	0.593pF
Capacitance at -6V bias C_r	0.300pF
Junction Grading Coefficient (M)	0.333
Package Capacitance C_{pk}	0.090pF
Series Resistance R_s	1.20Ω
Package Inductance L_{pk}	0.350nH

**Figure 3.4:** SRD model employed in ADS Simulation

The MCL for SRD employed is 8ns and forward resistance (R_f) was found to be 1.04Ω corresponding to forward bias current of 25mA for which R_s is 1.2Ω according to the SRD datasheet. Also, the V_j was measured using a multimeter to be 0.89V and has been included in the modeled SRD. A linear grading has been assumed for junction of the SRD and hence, a grading coefficient of 0.333 has been incorporated in the model. The parasitic parameters viz. package capacitance($C_{pk} = 0.09\text{pF}$), package inductance ($L_{pk} = 0.35\text{nH}$) and series resistance ($R_s = 1.2\Omega$) have been included in the model by taking the mentioned values as in datasheet of the diode in picture. The junction resistance and capacitance were replaced by a diode model with the parameter values

specified by the manufacturer. C_{pk} and L_{pk} are the parasitics due to the package.

3.4 Analysis of SRD Model

The model designed in ADS 2009 was analyzed by simple circuit designs. The circuit for the same is shown in Figure 3.5.

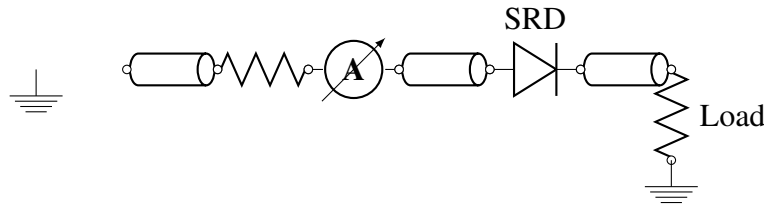


Figure 3.5: Model testing circuit

The current waveforms corresponding to square wave input and sinusoidal input are shown in Figure 3.6. and Figure 3.7 respectively.

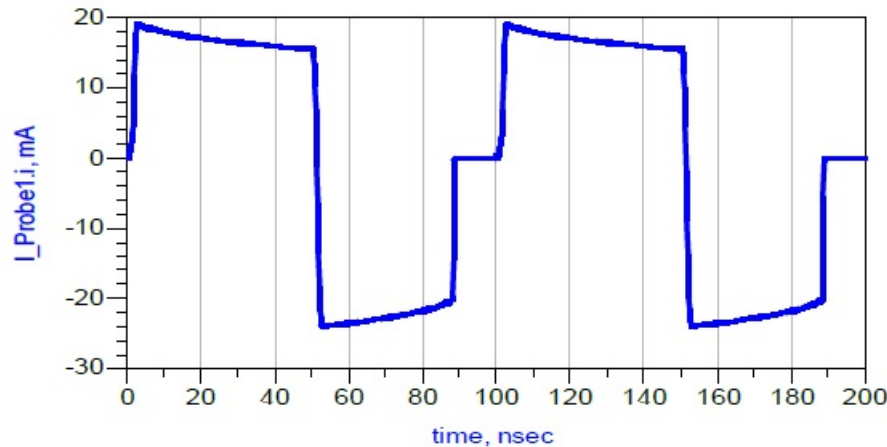


Figure 3.6: Output voltage waveform for a square wave input

The waveforms are current waveforms through the DUT and they very much stand up to the expectations. The output (for $t \leq 50$ ns) corresponding to square wave signal shows the forward charging current, and the gradual decay during the forward conduction shows the process of attainment of equilibrium between the charge accumulation and recombination. The current waveform (for 50 ns $\leq t \leq 88$ ns) represents the reverse storage conduction phase when injection of charges has stopped and the injected ones are being removed. When the charges are removed completely, the current value drops to zero without any turn-on transient rounding effect. The absence of rounding effect is

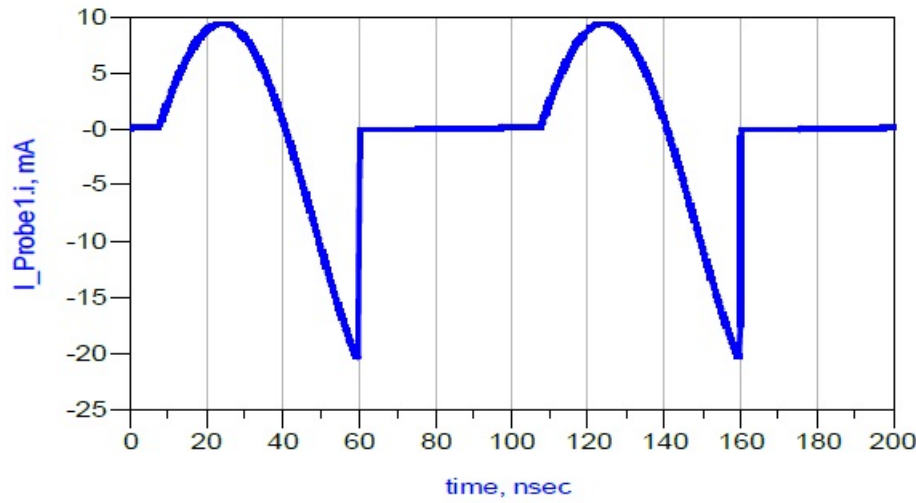


Figure 3.7: Output voltage waveform for a sine wave input

due to the zero residual charges, as they have not been included in the model. Now, the current waveforms are nearly same as predicted and reported in previous works for the square wave input [40], [41] and sinusoidal excitation [5], [9], [17].

Chapter 4

Circuit Design and Simulation

Preface

This chapter discusses the designing procedure and the design of the pulse generators. Each segment of the design has been separately discussed and analyzed. Design equations, figures, tables and simulation results have also been added.

The most commonly used component for UWB pulse generation has been the Step Recovery Diode which is also known as the snap diode for its abrupt switching characteristics. It generates a step signal that acts as the only ingredient for pulse formation. This step signal is rich in harmonic content and the risetime of this step decides the maximum frequency content of the pulse that can be constructed.

4.1 Pulse Generation Concept

Various pulse generator designs have been reported till date. The designing work can be divided into two broad categories as shaping a step signal to obtain a pulse using passive circuit networks and harmonic generation where the input is a sinusoidal signal. The first method has been taken up here as per the application it is intended to be used for. The other concept of pulse generation has been exploited and researched to a great extent in history and is still going on. Considering the pulse generation in the time domain, using an SRD, we can say that it seems to generate a ramp-like pulse instead of a Gaussian pulse. The pulse generation concept mostly exploited, uses a reverse transmission line to obtain an out-of phase step w.r.t. the one generated by the SRD. The pulse formation using the concept of reverse transmission line is explained in detail to pinpoint the source of distortion. This concept of pulse formation has the capability to give equal risetime and falltime. This is graphically described in Figure 4.1.

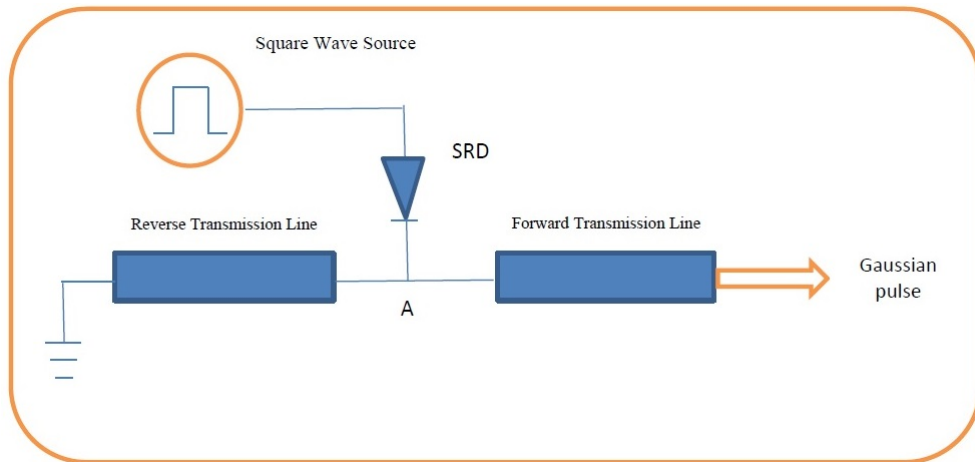


Figure 4.1: SRD Pulse Generation Concept

A reverse transmission line is a shorted stub of appropriate length to introduce an apt amount of delay. At point A, the ramp-like pulse produced by the SRD splits into two, with one traveling down the reverse transmission line and the other along the forward transmission line. The ramp-like pulse moving down the reverse transmission line bounces back with opposite polarity and is time delayed as it has to travel the length of

the short-stub. The reflected step comes back to point A and splits into one travelling towards the source (fast leakage step) and the other going for the load. The one going for load combines with the original step and forms the Gaussian pulse, whereas the one that is backtracking towards the source is reflected again from the source and distorts the Gaussian pulse as shown in Figure 4.2.

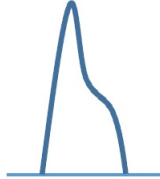


Figure 4.2: Step waves' combination to the right of point A

The fast leakage step needs to be exterminated by placing some network in its path. This problem is dealt with strictly in this work and it will be explained at a later stage. Now, when these distortion sources are taken care of, the FWHM of the Gaussian pulse is proportional to the delay introduced (T_d) which is determined by the length of the short circuited transmission line (L_{TL}) and the material medium and is analytically computed using (4.1.1).

$$T_d = \frac{2L_{TL}}{v_p} \quad (4.1.1)$$

Phase velocity (v_p) of the signal is determined by the nature of the material used and is analytically estimated using (4.1.2).

$$v_p = \frac{c}{\sqrt{\epsilon_e}} \quad (4.1.2)$$

The effective dielectric constant ϵ_e depends on factors like structure and dimension of the transmission line. For a microstrip line (the transmission line technology employed here) having conductor thickness, w_m dielectric height, d the effective dielectric constant can be approximated as in (4.1.3).

$$\epsilon_e = \frac{\epsilon_r + 1}{2} + \frac{\epsilon_r - 1}{2 * \sqrt{1 + \frac{12d}{w_m}}} \quad (4.1.3)$$

4.2 Design Description

The source being used for the Gaussian pulse and Monocycle pulse generation is a pulse generator. The signal source is Agilent's waveform generator 33220A which is capable of generating bipolar square wave signal. The laminate being used is Roger's RO4350B,

having the properties shown in Table 4.1.

Table 4.1: Specifications of RO4350B Laminate

Dielectric constant	3.66
Dielectric height	0.508mm(20 mil)
Conductivity	5.96×10^7 S/m
Loss Tangent	0.0037
Conductor Thickness	0.035mm(1.378mil)
Relative Permeability	1

4.2.1 Gaussian Pulse Generator Circuit

The designed Gaussian pulse generator circuit has been explained here by parting it into three sections viz. step generator, 3dB attenuator and pulse shaper. A block diagram representation of the Gaussian pulse generator circuit (designed and simulated in ADS 2009) is shown in Figure 4.3.

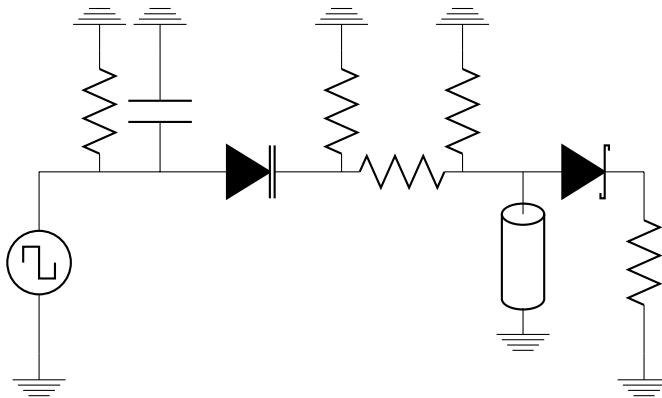
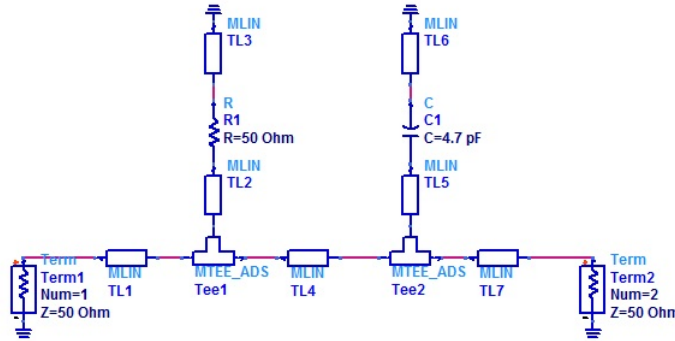


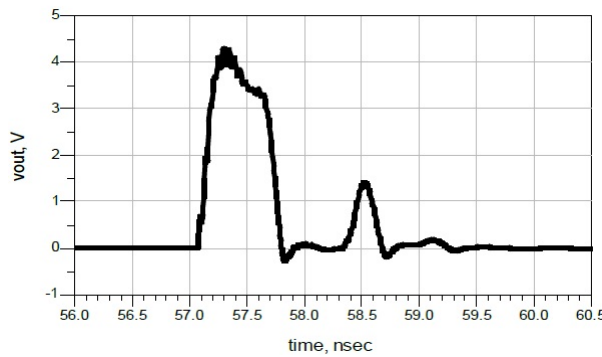
Figure 4.3: Gaussian pulse generator circuit

Step-generator

The Step-generator section consists of an input-matching network [51] to reduce distortions and an SRD in series mode to produce step signals with low risetime. Analyzing the need of the input matching circuit (Figure 4.4), it is certain that the fast leakage step due to which the Gaussian pulse gets deformed needs to be bypassed, as explained in section 4.1 and shown in Figure 4.2. The input matching network employed is an RC low-pass filter to allow only the trigger signal pass through to SRD. The fast leakage step reflected back from the shorted end of the reverse transmission line and coming towards the source is effectively bypassed to the ground. This vital addition has reduced the distortions in the required Gaussian pulse to a large extent.

**Figure 4.4:** Input Matching Circuit

To get a clear idea of the effect of adding the input matching network, the Gaussian pulse generator circuit was simulated without the network and compared graphically with the desired Gaussian pulse. The Gaussian pulse with the effect of input matching network included is shown in Figure 4.5.

**Figure 4.5:** Pulse generator output with no input matching circuit

Now, the modeled SRD has been included which provides the step signals or building blocks of our Gaussian pulse. The SRD employed has an intrinsic transition time of 60ps, as specified by the manufacturer. The SRD when placed in the pulse generator circuit shows a larger transition time which is the characteristic property of the whole circuitry. This transition rise time of the generator circuit is defined as the time during which SRD changes its impedance states within the circuit. It is dependent on the diode's intrinsic transition time, the circuit constraints and the level of stored charge. The diode's intrinsic transition time along with circuit risetime will decide the generator circuit's transition time according to (4.2.1).

$$t_{grt} = \sqrt{t_{crt}^2 + T_t^2} \quad (4.2.1)$$

In the above equation, t_{grt} represents the generator circuit's rise-time, T_t is the diode's

intrinsic transition time and t_{crt} is the circuit's rise time that depends on the diode's reverse bias capacitance, C_{dr} which is the total capacitance of diode in reverse bias (including the package capacitance, (C_{pk}) and equivalent resistance (R_{eq}) of source and load resistance in parallel (25Ω for a 50Ω system).

For 10% – 90% rise time t_{crt} is given by,

$$t_{crt} = 2.2 * R_{eq} * C_{dr}$$

For 20% – 80% rise time t_{crt} is given by,

$$t_{crt} = 1.4 * R_{eq} * C_{dr}$$

The plot showing voltage across the SRD in the generator circuit is shown in Figure 4.6.

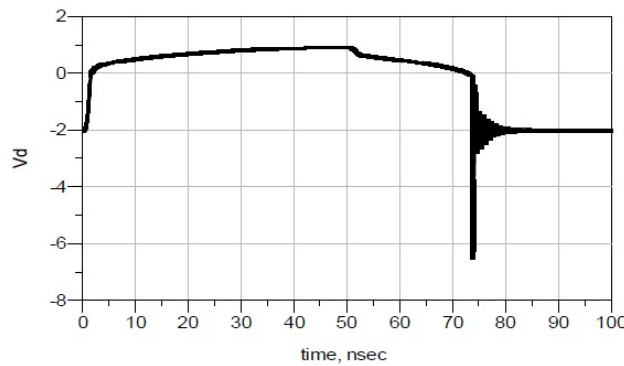


Figure 4.6: Voltage across SRD

The modeled diode transition time when placed in the generator circuit, t_{grt} was found out to be 90ps.

3dB Attenuator

The 3dB balanced resistive attenuator is a symmetrical π -network with resistive lumped elements for UWB performance. It is employed to reduce the impedance mismatch and reduce the distortions by attenuating the fast leakage step while returning from stub and again when it is reflected from the source. So, the step generated by SRD (the wanted one) is attenuated once but the unwanted fast leakage step is attenuated twice.

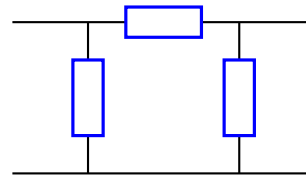


Figure 4.7: Conventional resistive symmetric π -network

The design equations can be derived using Z-matrix and S-matrix representation of conventional π -network (Figure 4.7) with:

$$S_{11} = S_{22} = 0 \quad (4.2.2)$$

$$S_{21} = S_{12} \quad (4.2.3)$$

Converting dB (logarithmic ratio) representation to linear ratio,

$$S_{21} = 10^{-\frac{S_{21}(dB)}{20}} \quad (4.2.4)$$

Now the Z-parameters for the network are:

$$\begin{aligned} Z_{11} = Z_{22} &= \frac{R_X(R_Z + R_X)}{R_Z + 2R_X} \\ Z_{21} = Z_{12} &= \frac{R_X^2}{(R_Z + 2R_X)} \end{aligned} \quad (4.2.5)$$

The S-parameters are:

$$S_{11} = S_{22} = \frac{(Z_{11}^2 - Z_0^2 - Z_{21}^2)}{(Z_{11} + Z_0)^2 - Z_{21}^2} = 0 \quad (4.2.6)$$

The above equation using (4.2.5) can be written as,

$$R_Z = \frac{2Z_0^2 R_X}{R_X^2 - Z_0^2} \quad (4.2.7)$$

$$S_{21} = S_{12} = \frac{2Z_{21}Z_0}{(Z_{11} + Z_0)^2 - Z_{21}^2} \quad (4.2.8)$$

Simplifying the above equation using (4.2.5),

$$S_{21} = \frac{\frac{2R_X}{R_Z}}{\left(\frac{R_X}{Z_0} + 1\right)^2} \quad (4.2.9)$$

Substituting R_Z from (4.2.7) into (4.2.9),

$$R_X = Z_0 * \frac{(1 + S_{21})}{(1 - S_{21})} \quad (4.2.10)$$

Here, S_{21} is 3dB which corresponds to $|S_{21}| = 0.708$. Taking source impedance,

$Z_S=50\Omega$ for a system of $Z_0=50\omega$, the value for shunt resistances were obtained as $R_x = 292.46\Omega$ and the series resistance was found out to be $R_z = 17.61\Omega$. Fine tuning was done for the best simulation output and the values were settled at $R_X = 330\Omega$ and $R_Z = 18\Omega$ respectively. The tuned attenuator gives an attenuation of 2.65dB. The job of attenuator (Figure 4.8a) in this application is to attenuate the fast leakage step but it will affect the wanted step also which needs to be minimized such that the minimization does not distort the output waveform much. Hence, a balance between the attenuation and distortion is needed. So, tuning was done to obtain a best output which explains the difference between the resistance values calculated and values in the fabricated design. The wideband 3dB attenuation performance is evident from the S_{21} variation with frequency shown in Figure 4.8b. The exact shape of S_{11} and S_{22} ensured the obvious symmetry of the network.

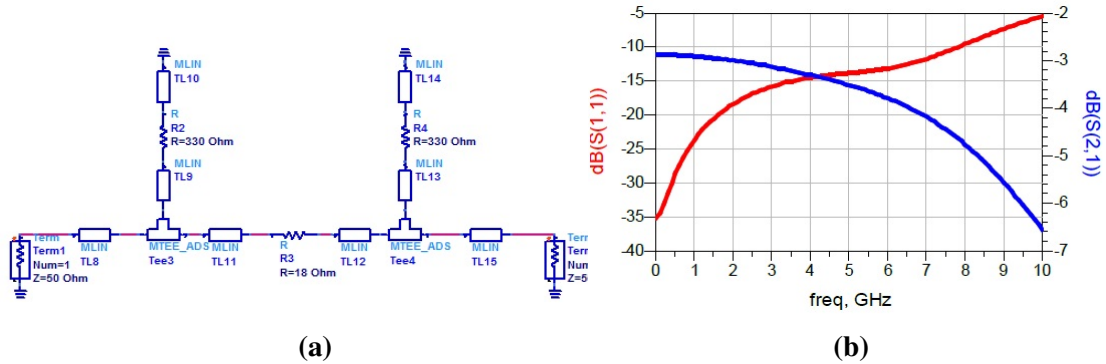


Figure 4.8: (a) The implemented attenuator (b) Frequency response

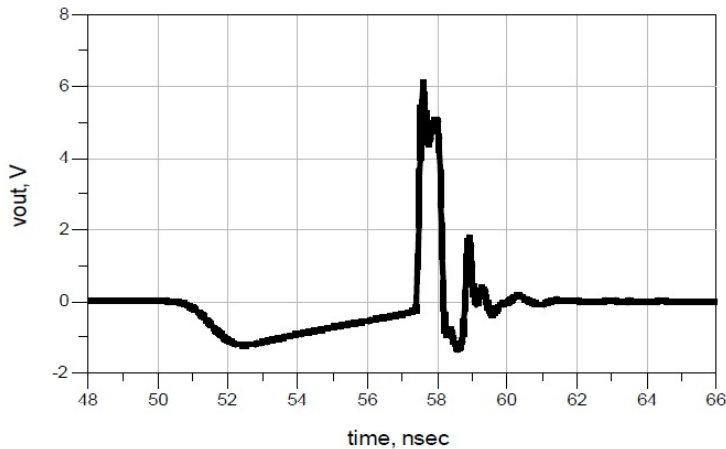


Figure 4.9: Gaussian pulse generator output without attenuator

Now, to get a clear picture of advantages of the attenuator, the Gaussian pulse generated without attenuator (Figure 4.9) is compared with the desired Gaussian pulse.

Pulse shaper

This section consists of a shorted stub ($Z_L=0$) in shunt configuration and a Schottky diode (SD) in series. The shorted stub plays the role of a reverse transmission line, as it is the pathway for the reflected waves V^- travelling in the reverse direction. These waves are 180-degrees out-of phase w.r.t. the incident waves V^+ , as the reflection coefficient Γ is -1 which is apparent from (4.2.11).

$$\Gamma = \frac{V^-}{V^+} = \frac{(Z_L - Z_0)}{(Z_L + Z_0)} \quad (4.2.11)$$

Length of short stub (L_{TL}) used for Gaussian pulse formation is estimated numerically, for required pulselwidth using (4.1.1). The designed circuit employs a substrate having permittivity of $3.66\epsilon_0$ which has an effective dielectric constant of 2.84 corresponding to $w_m=1.08\text{mm}$ and $d=0.508\text{mm}$. The wave velocity, v for this material is $1.77 \times 10^8 \text{ms}^{-1}$ which corresponds to delay of 100ps for a stub of length, $L_{TL} = 8.84\text{mm}$. The delay to be introduced will be same as the generated pulse's FWHM, this equality is illustrated in Figure 4.10a and Figure 4.10b. The reason behind this choice of targeted delay of 100ps is the diode's transition time of 90ps (0 – 100%) when placed in the generator circuit. Theoretically, for least flattening of the peak of the Gaussian pulse, the delay introduced can be assumed to be around 100ps.

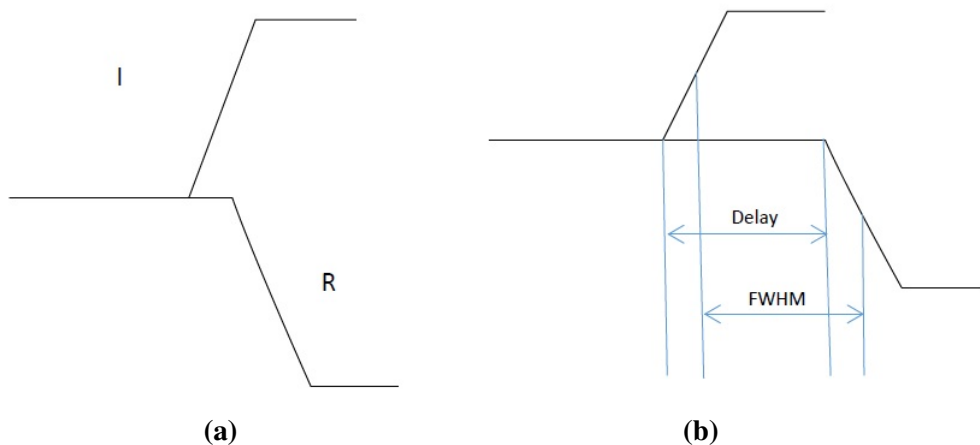


Figure 4.10: (a) Incident step and reflected step (b) Showing equality of Delay and FWHM

Trade-off in using a stub for pulse formation is the generation of bipolar ringing that limits resolution of sensing radars. The bipolar ringing is shown in Figure 4.11 which shows the output voltage waveform of the Gaussian pulse generator circuit without any measure to remove it. The other component in this pulse shaper section is a Schottky Diode (SD). An SD is a fast switching device and is used as half-wave rectifier to chop-

off the negative portion of the high frequency ringing tail and pass the positive polarity Gaussian pulse intact.

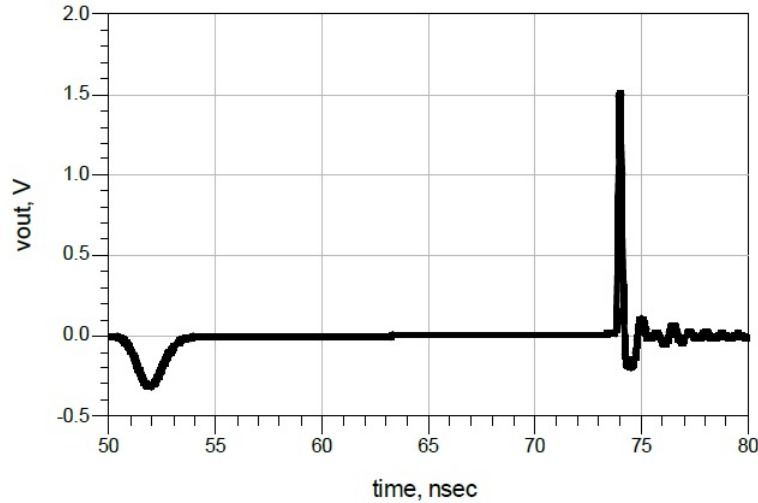


Figure 4.11: Gaussian pulse generator output without the rectifier

The Gaussian pulse generated is having a high level of ringing ($-17.81dB$) and from the figure above, the bipolar nature is also clear. They can be reduced or removed by using a half-wave rectifier or diode having faster switching capability. This necessity forced us to use a Schottky diode as a half-wave rectifier. After this stage a well behaved Gaussian pulse is obtained as shown in Figure 4.12 along with its spectrum in Figure 4.13.

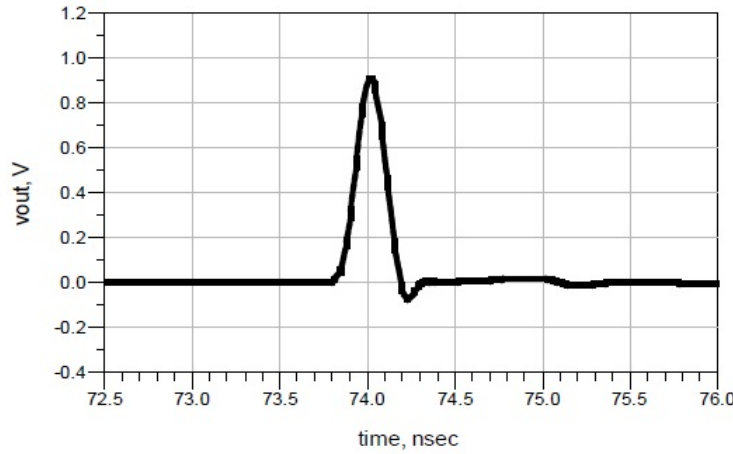
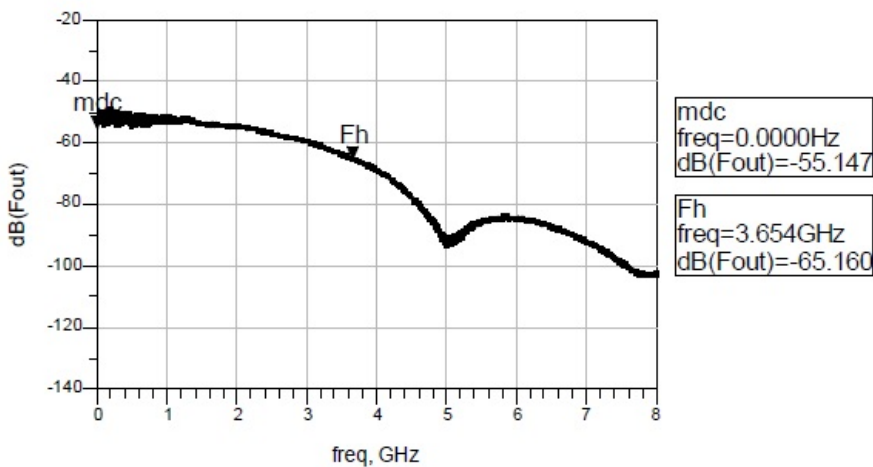


Figure 4.12: Output with source matched and attenuator and rectifier in place

The properties of Gaussian pulse generated in simulation are showcased below in Table 4.2.

Table 4.2: Properties of the Simulated Gaussian Pulse

Characteristic Property	Value
Peak Value	0.91V
Rise-time (10% – 90%)	119ps
Fall-time (90% – 10%)	116ps
FWHM (50% – 50%)	190ps
Ringing	-22dB
Peak Repetition frequency	10MHz
10dB-Bandwidth	3.6GHz

**Figure 4.13:** Spectrum of the simulated Gaussian pulse

4.2.2 Monocycle Pulse Generator Circuit

The generated Gaussian pulse can be transformed into a monocycle by two ways. One way is to Fold, Shift and Add which is exactly the process of formation of monocycle that employs a shunt shorted stub. This method is very prone to ringing as reflections will be introduced. Moreover, the FWHM of the monocycle obtained by this method will be more than twice compared to the other one which differentiates the Gaussian pulse to get a monocycle. A differentiator network has been added which differentiates the Gaussian pulse in time domain and in the frequency domain it can be said that it reshapes the spectrum of the Gaussian pulse by removing the low frequency contents. The differentiator is as shown in Figure 4.14a and the component values have been tuned to give the best output. The frequency response of the designed differentiator is shown in Figure 4.14b. The return loss curve shows a dip in the low frequency region but the high insertion loss in this range evidently results in suppression of the low frequency components.

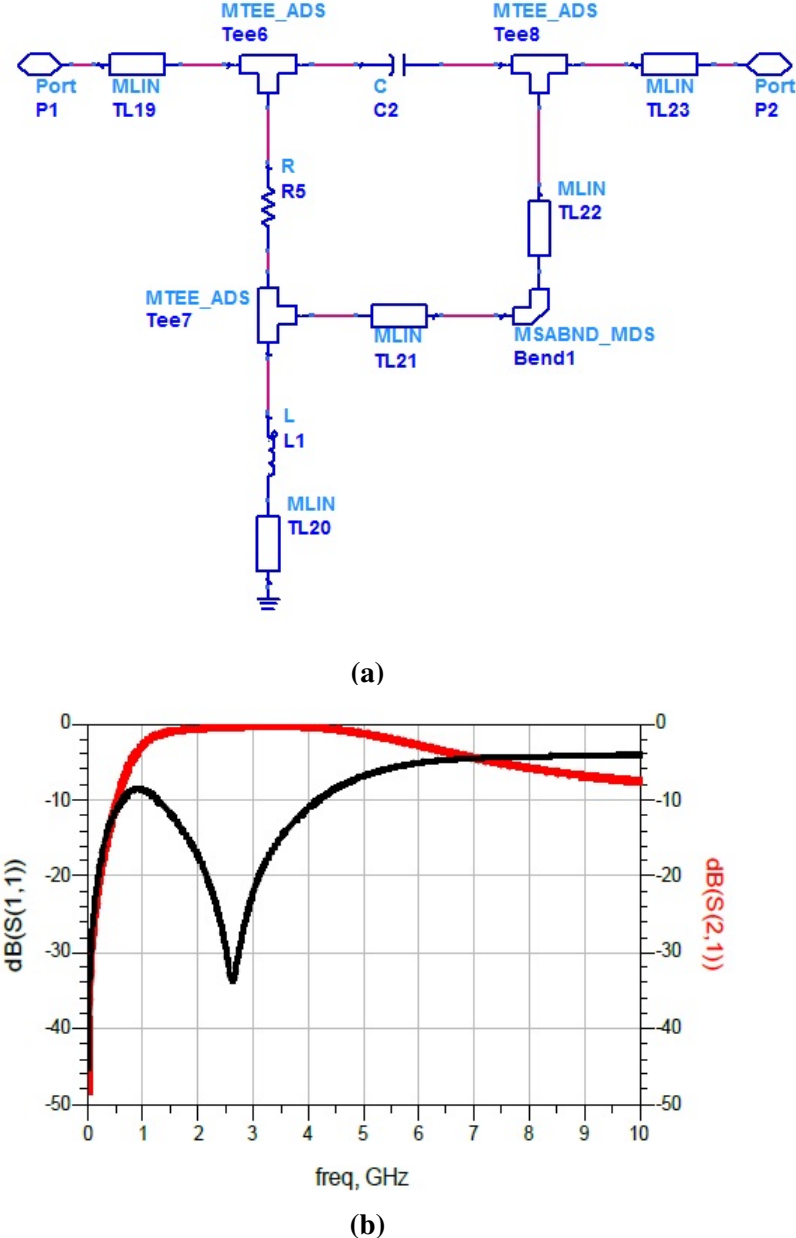


Figure 4.14: (a) Differentiator network (b) Frequency response of the differentiator

The differentiator network [52] is solely responsible for shaping the Gaussian pulse into a monocycle by differentiating the Gaussian pulse in time domain. The differentiating network comprises of a capacitance of 4.7pF , a resistance of 50Ω and an inductance of 2.2nH . Differentiation is mainly accomplished by the capacitor, C_2 whereas the other components like resistor, R_5 regulates the time constant of the differentiator and the inductor, L_1 can be understood as a bypass route to ground for the unwanted, low fre-

quency components. The differentiator here is a network of lumped elements and the network is not purely capacitive so it is a bandpass filter. This is justified by the bandpass behavior shown by the network. This bandpass behavior is indeed needed for a pulse generator design so that the unwanted high frequency ringing components can be suppressed. Now, the operation of obtaining a monocycle pulse from a Gaussian pulse can also be viewed as a bandpass operation. The frequency response of the network employed, looks like that of a band-pass filter which removes the low frequency components from the Gaussian pulse and the high frequency ringing portion. The simulated 3dB-bandwidth of the band-pass filter is 3GHz. Preceding this differentiator network with the Gaussian pulse generator circuit designed, we obtain the monocycle pulse generator which is represented using block diagrams as shown in Figure 4.15. The monocycle generator circuit's output voltage waveform is shown in Figure 4.16 along with its spectrum in Figure 4.17.

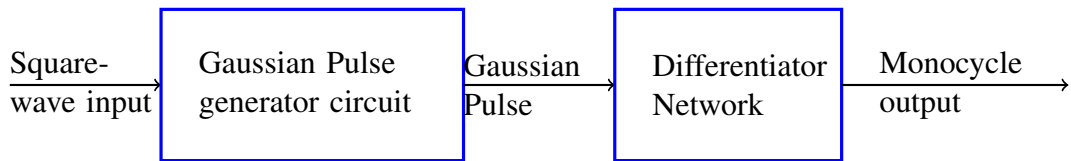


Figure 4.15: Monocycle Pulse generator circuit

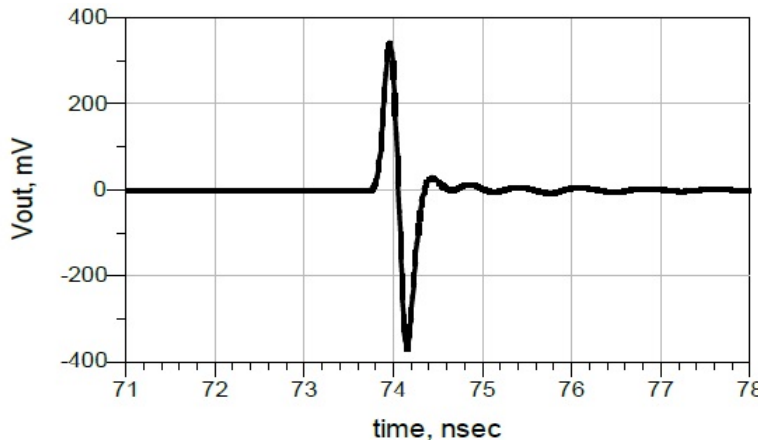


Figure 4.16: Monocycle output

The markers in the spectrum plot show the signal strength at the respective frequency points. Marker ' F_p ' denotes the peak signal strength whereas ' F_1 ' and ' F_2 ' are for the 10dB down points in the lower frequency bound and upper frequency bound respectively. The properties of generated monocycle are tabulated in Table 4.3. The monocycle pulse obtained has a good shape and a low ringing which makes it an acceptable simulation result and gave the thrust to go for fabrication.

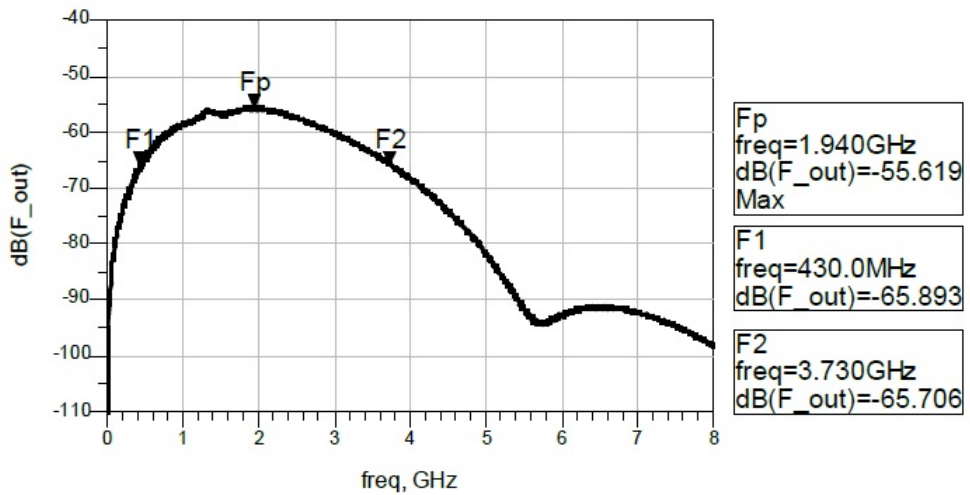


Figure 4.17: Spectrum of the Monocycle pulse

Table 4.3: Properties of the Simulated Monocycle Pulse

Characteristic Property	Value
Peak to peak voltage	0.675 V
FWHM	355 ps
Ringing	-25 dB
Peak Repetition frequency	10 MHz
10dB-Bandwidth	3.3 GHz
Fractional Bandwidth	158%

4.2.3 Frequency Domain Analysis

As mentioned earlier, in this chapter, the designed pulse generator circuits are analyzed in frequency domain for reliability and stability check.

First, we analyze the ingredient of the Gaussian pulse which is the step signal generated by the SRD. The step signal generated by the SRD has spectrum as shown in Figure 4.18. The high signal strength is witnessed at frequencies near the dc and presence of relatively low power but a good amount at higher frequencies is as per the need. This signal, rich in harmonic content, is passed through a network comprising of a 3dB attenuator and a shorted shunt stub. The step signal after passing through, gets shaped into a Gaussian pulse. The attenuator is a vital part of the pulse generator network, the job of which can be understood in time domain as, attenuating the unwanted fast leakage step reflected by the stub and going towards the source.

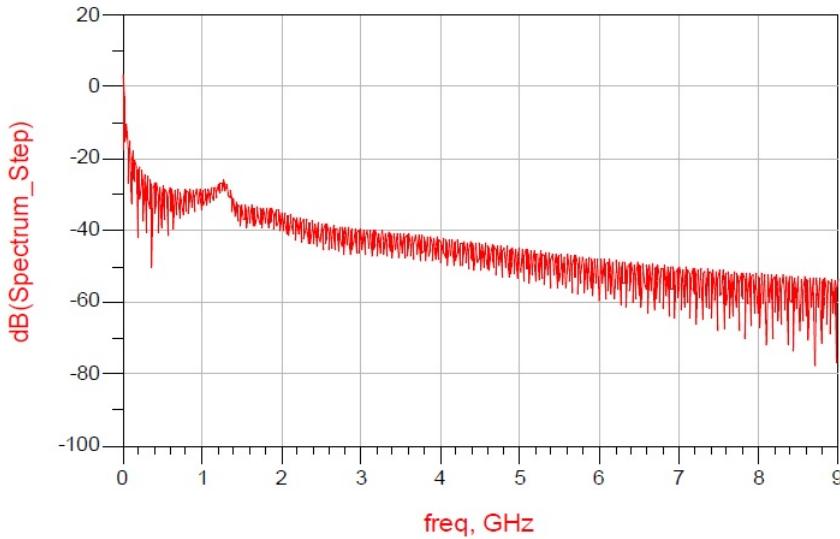


Figure 4.18: Spectrum of the step signal generated by SRD

In frequency domain, it performs the task of impedance matching without which reflections would be high and distortions in the output even higher. The vitality of the attenuator is checked by performing the S-parameter simulation of the network without attenuator. The results are plotted in Figure 4.19 along with spectrum of the signal obtained without the attenuator in Figure 4.20. Now, the network including the attenuator is simulated and the frequency response is shown in Figure 4.21.

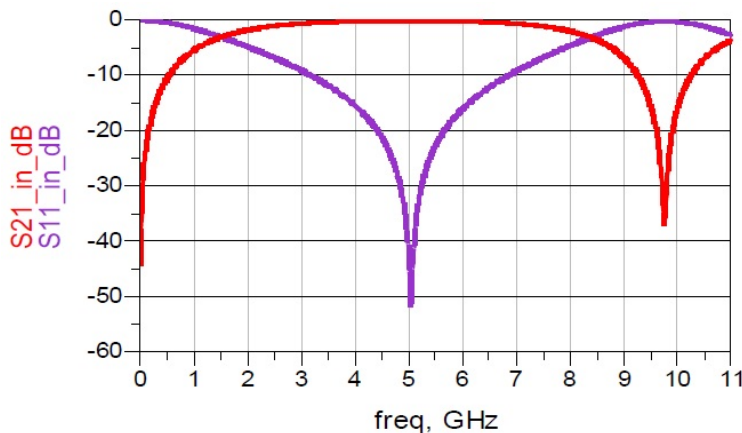


Figure 4.19: Frequency response of the network without attenuator

Comparing the response in Figure 4.19 and Figure 4.21, it can be pointed out that the circuit simulated without the attenuator shows impedance match over a bandwidth of 3GHz whereas, with the attenuator in place it increases to 5.33GHz. Moreover, on extending the simulation frequency range, it was witnessed that the network without

attenuator showed multiband bandpass response. This will introduce high frequency ringing and in comparison, the network with attenuator showed severe attenuation in the same range. In recently reported works [87], frequency domain circuit designing was undertaken where it was shown that Gaussian pulses and monocycles can be generated by using bandpass filter sections.

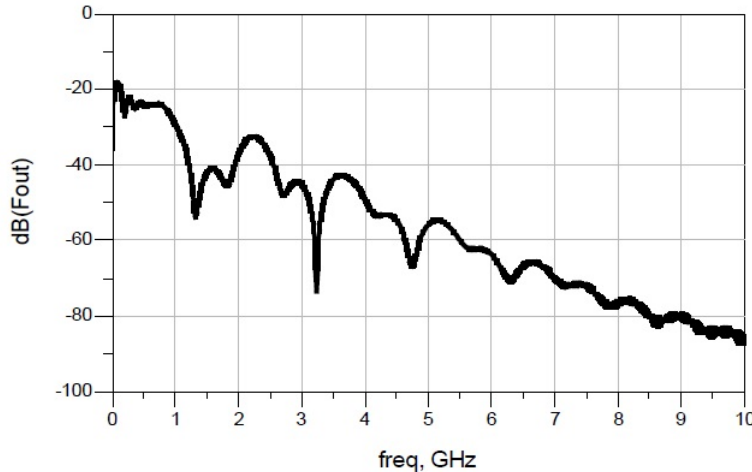


Figure 4.20: Spectrum of the signal obtained without attenuator

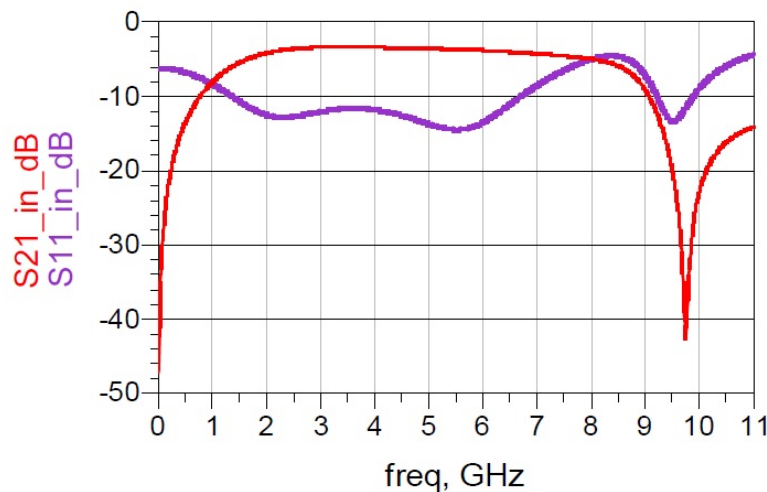


Figure 4.21: Frequency response of the Gaussian pulse shaping section

The differentiator, designed to shape the Gaussian pulse into monocycle, has also confirmed bandpass behavior. Hence, it can be concluded that generating a Gaussian pulse from a step signal is a bandpass operation and shaping a Gaussian pulse into a Monocycle is also a bandpass operation. Another important parameter that needs attention is the group delay of the frequency components passing through the bandpass filter. Ideally,

the group delay should be independent of frequency or the filter should be a linear phase filter for least distortion. The phase and group delay of the designed bandpass filter is shown in Figure 4.22 and Figure 4.23 respectively.

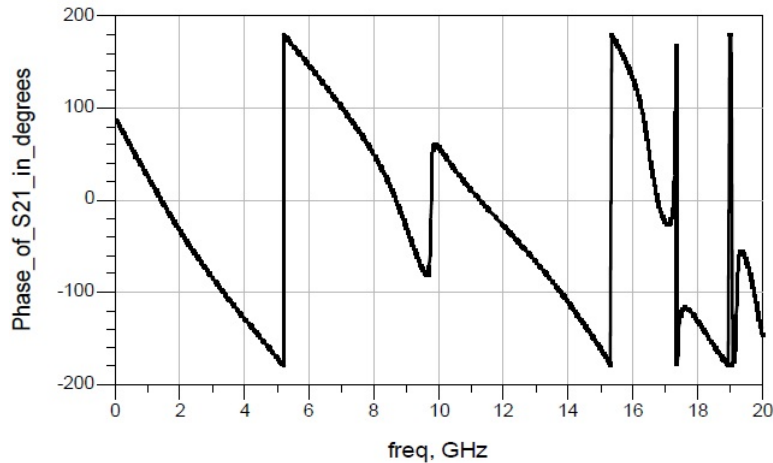


Figure 4.22: Phase of transfer characteristics

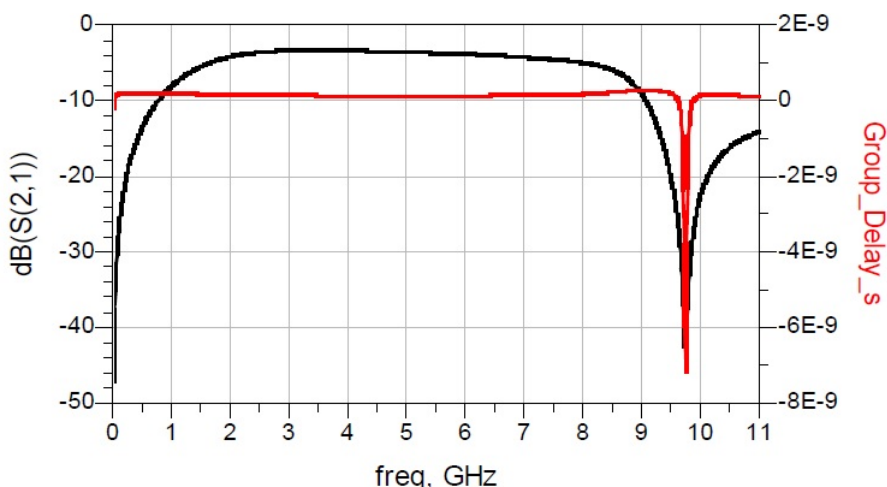


Figure 4.23: Simulated circuit's S_{21} and group delay

The constant value of group delay is clear from the plot shown above. So, it is affirmative that the circuits designed here are acceptable.

Chapter 5

Fabrication and Measurement

Preface

In this chapter, the measurement results are presented and compared with the simulation results. Figures showing and comparing the results and tables are also included.

5.1 Fabrication

The microstrip layout of the designed pulse generators was drawn in the same platform (ADS2009). Both the circuits' layout was drawn together so that they can be fabricated on a single board. The layout for the same is shown in Figure 5.1.

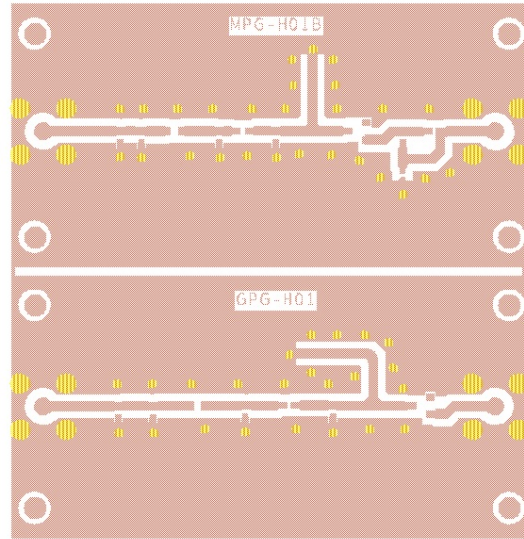


Figure 5.1: Layout of the circuits

The circuit in the upper half of the layout is the monocycle generator and the Gaussian pulse generator is in the other half. The generators were fabricated in the labs of HCL, Chennai. The measurements were taken using Tektronix TDS6124C Oscilloscope. The fabricated circuit's snap is shown in Figure 5.2.

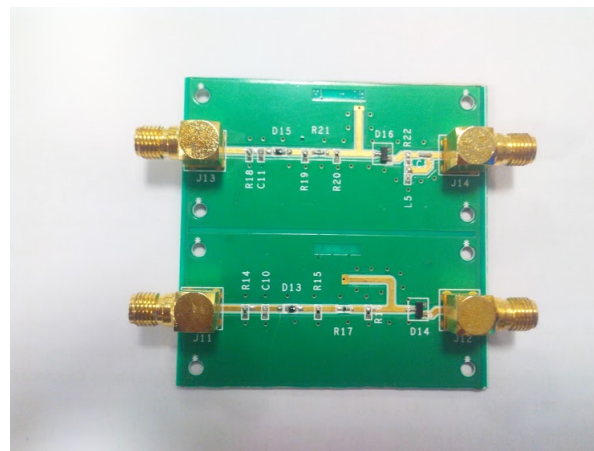


Figure 5.2: Photograph of fabricated circuits

5.2 Measurement Results

The generator circuits were tested using Agilent's 33220A waveform generator. The source signal is shown in Figure 5.3.

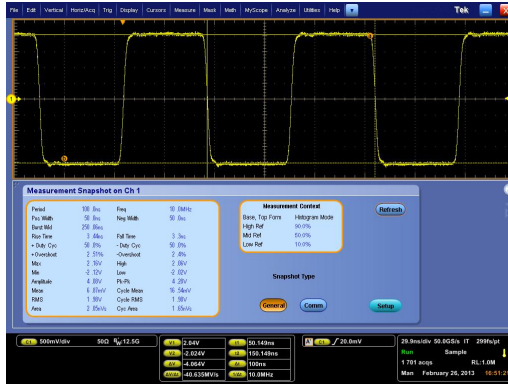


Figure 5.3: The 10MHz source signal

The signal is a bipolar square wave of 10MHz and with voltage levels at 2V and -2V. The rise time and fall time were set to 3ns but the observed risetime of the input was found to be 3.44ns and the falltime was 3.3ns. This dispersion can be attributed to the surfacing of inductive and capacitive parasitics in the cable. This dispersion effect was taken care while doing the simulations in ADS 2009 by setting the type of rising edge and falling edge of input signal edge to 'erf' in the parameter entry mode dropdown menu which makes the risetime and falltime, an approximation of the real behavior.



Figure 5.4: (a) The generated Gaussian pulse and (b) its Spectrum

Snapshots of the generated Gaussian pulse and monocycle in time domain are shown in Figure 5.4a and Figure 5.5a respectively. The spectrum of the generated signals are in Figure 5.4b and Figure 5.5b.

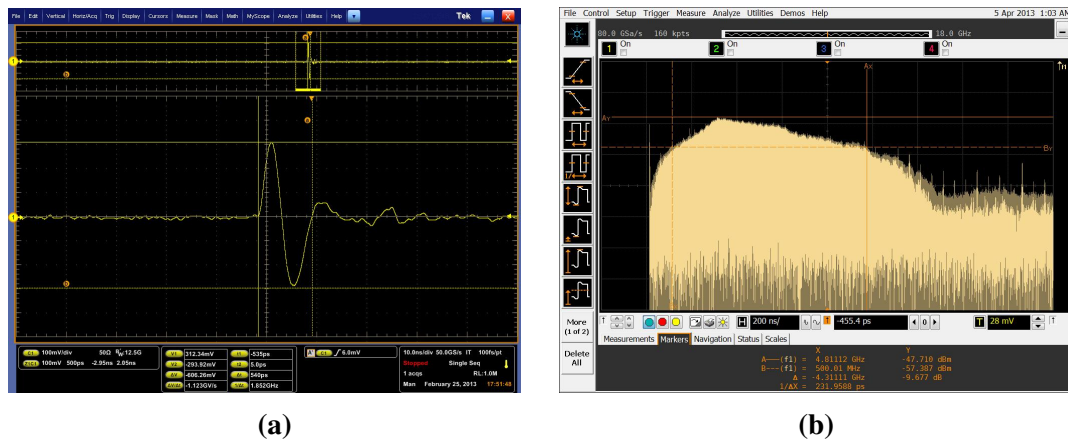


Figure 5.5: (a) The generated monocycle and (b) its Spectrum

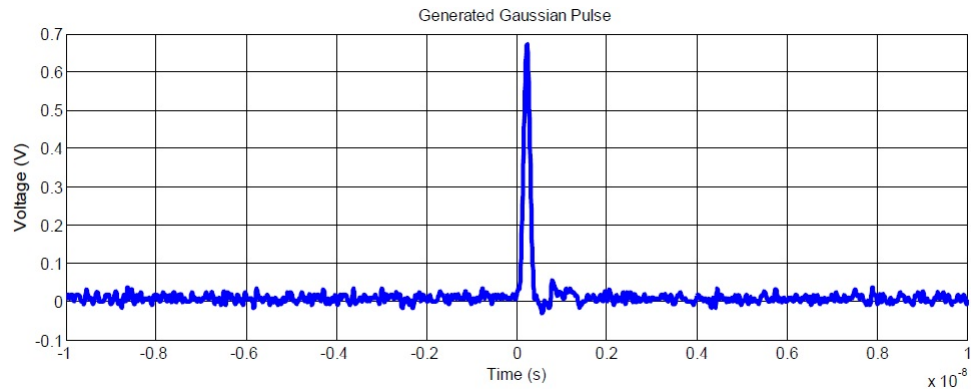


Figure 5.6: Generated Gaussian Pulse plotted in MATLAB 2012B

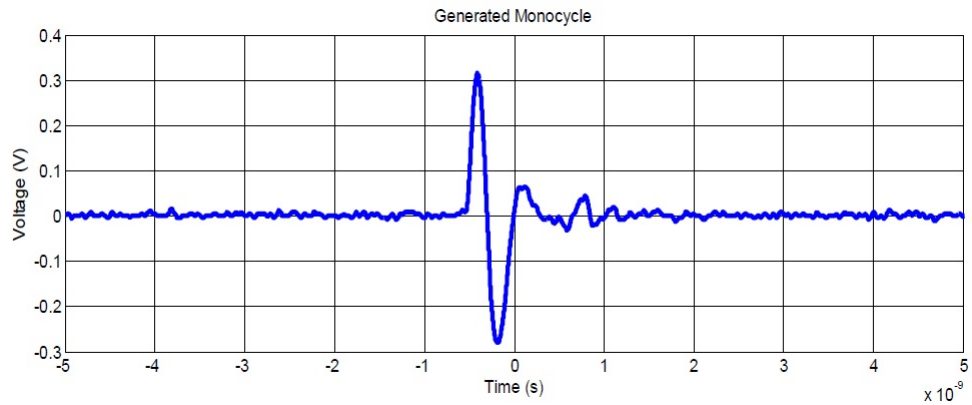


Figure 5.7: Generated Monocycle plotted in MATLAB 2012B

The generated signals were found to be insensitive to increase in input PRF from 1MHz to 100MHz. The pulses were generated at 10MHz as a train to facilitate the periodicity

check of the circuits, whereas here it is shown for a single period. The pulses generated were also plotted in MATLAB 2012 using data-files generated by the oscilloscope. The time window was truncated to magnify the pulses for a better view and clarity for comparison. The Gaussian pulse plot is shown in Figure 5.6 and the monocycle in Figure 5.7.

5.3 Reliability Analysis

Next, the reliability of the pulse generator circuits was tested w.r.t. the non-uniform delay that creeps in and leads to variations in the periodicity of the signal by shifting the signal's instants from their respective ideal positions. These delays are analyzed in terms of statistical parameters like Standard deviation (σ), mean value (μ) and peak to peak deviation within a particular confidence interval. These non-uniform delays are best known as Random Jitter in high speed circuits. The jitter analysis plots are shown in Figure 5.8a and Figure 5.8b. The two plots show the Random jitter having Normal or Gaussian distribution(in blue). The metric parameters for the Gaussian distribution have been employed and the standard deviation or the root mean square value was seen to be 1.58ps. The mean values of the significant instants are mentioned in measured values' column of Table 5.1. The peak to peak variations in parameters in the table were witnessed to be 9.5ps within a confidence interval of 99.7%.

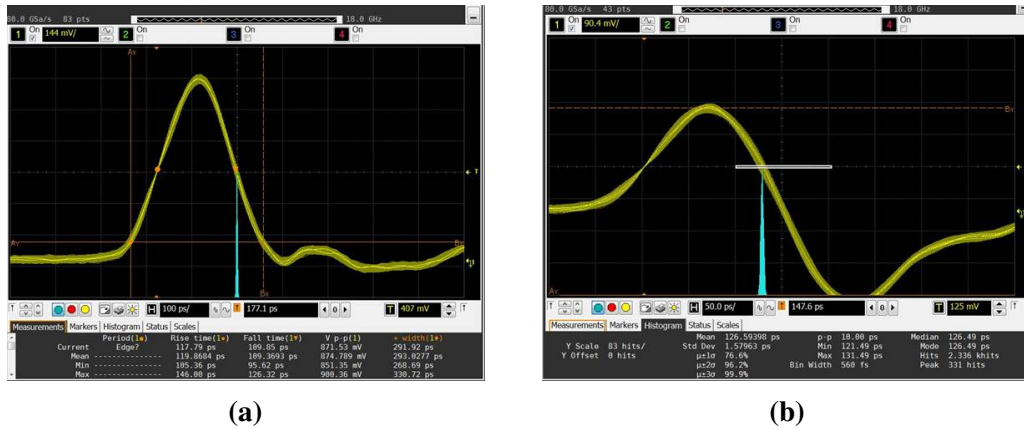


Figure 5.8: Jitter analysis in the (a) Gaussian (b) monocycle pulse generator circuits

The measuring parameters that are included in Table 5.1 can be enlisted and understood as:

- (a) Voltage is the peak voltage for Gaussian pulse and peak to peak voltage for monocycle,
- (b) Risetime and Falltime which correspond to the 10% point to 90% point and vice

versa,

- (c) FWHM for the Gaussian pulse has a literal meaning but for monocycle it stands for the duration between the 50% values for monocycle's envelope,
- (d) Duration specifies the time duration between the 10% levels of Gaussian pulse and 10% levels of the corresponding positive and negative peaks in case of monocycle,
- (e) RMS jitter,
- (f) Peak to peak jitter,
- (g) Ringing characteristic (in dB),
- (h) 10dB-Bandwidth of the signals,
- (i) Fractional Bandwidth (η), which is an important parameter along with the bandwidth to decide the UWB nature of a signal.

Table 5.1: Comparison between the Simulated and Measured Results

Parameters	Gaussian Pulse		Monocycle Pulse	
	Simulated	Measured	Simulated	Measured
Voltage (V)	0.91	0.87	0.68	0.60
Risetime (ps)	119	119	-	-
Falltime (ps)	116	109	-	-
FWHM (ps)	190	170	355	401
Duration (ps)	312	275	574	500
RMS Jitter (ps)	-	1.58	-	1.58
Jitter pk-pk (ps)	-	9.5	-	9.5
Ringing in dB	-22	-22	-25	-16
10dB-Bandwidth (GHz)	3.6	3.0	3.3	4.3
Fractional Bandwidth (η)	-	-	158%	162%
PRF (MHz)	10	1-100	10	1-100

Now, a graphical comparison between the simulated and measured signals is presented in Figure 5.9 and Figure 5.10. A considerable drop in amplitude of the generated signals was witnessed, which can be attributed to the approximate modeling of non-linear variation in junction resistance of the SRD. The length of short stub in simulated Gaussian pulse generator circuit is 9.29mm whereas for the realized one it is approximately 9.65mm.

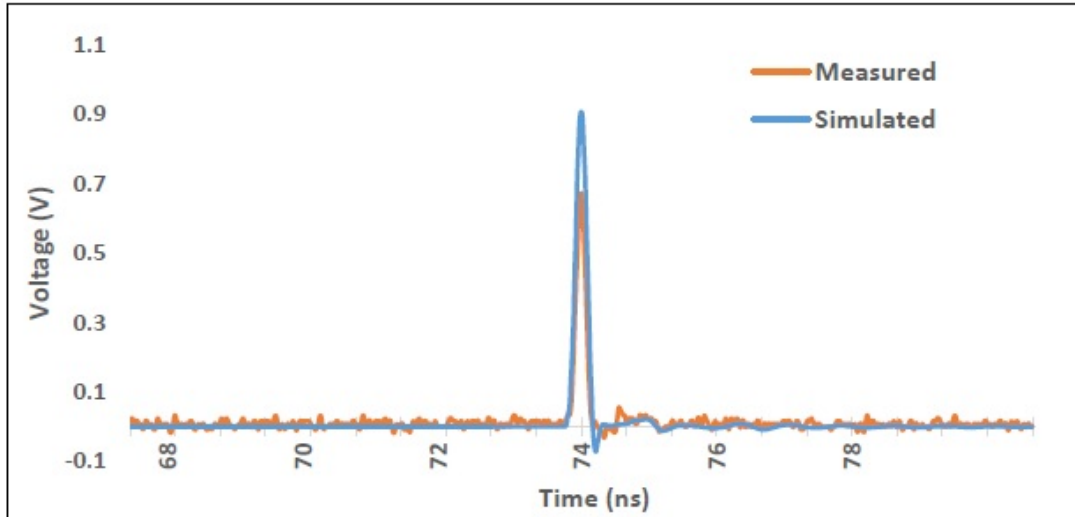


Figure 5.9: Comparison between simulated and measured Gaussian pulse

Also, the FWHM of simulated and measured Gaussian pulse is showing a difference of 20ps, which is most likely due to the microstrip bend introduced in the circuit. The bend introduces discontinuity reactance [88], reducing the effective length of the short stub which explains the difference in length of the stubs in simulated and realized circuit.

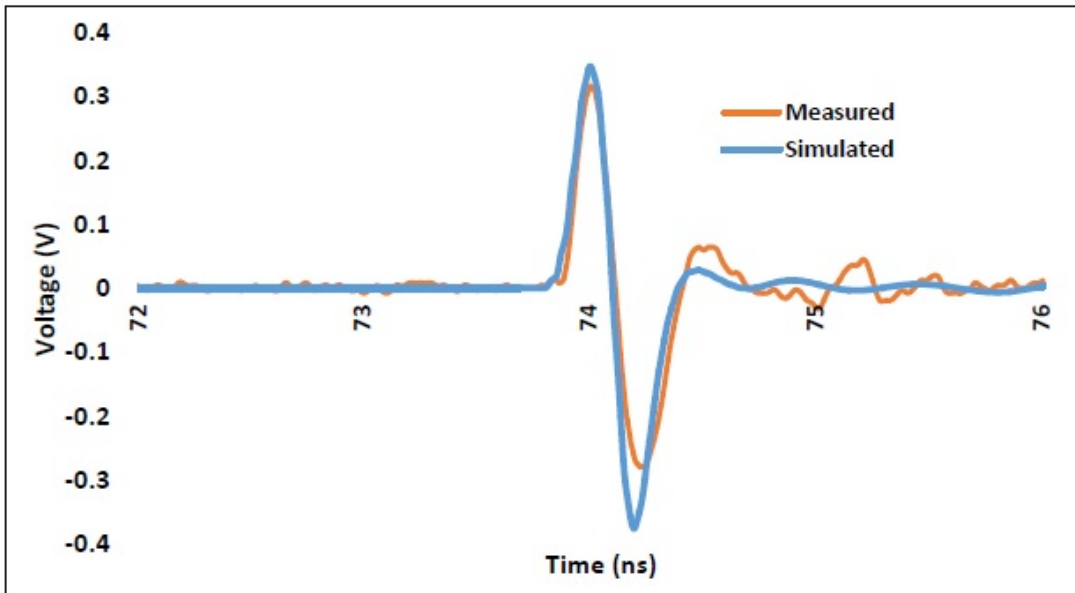


Figure 5.10: Comparison between simulated and measured Monocycle

Moreover, the short stub fabricated, includes via grounding which introduces inductive reactance and resistance [89]. The surfacing of these parasitics is also among the reasons

for the difference in length of stub in simulation and in the fabricated circuit. In case of the monocycle generator, the short stub length is 5.58mm in simulated circuit and 6.5mm in the realized one. The generated monocycle is having a remarkable fractional bandwidth of 162% which is far greater than η_{min} ($\eta_{min} = 20\%$) and a noteworthy bandwidth of 4.3 GHz. The generated Gaussian pulse is also having an UWB bandwidth (3.0 GHz). So, it is substantiated that the signal is having UWB characteristics.

5.4 Relative Performance Evaluation

The various pulse generator designs in literature are compared in Table 5.2 for performance evaluation in a relative sense. The works have been compared on various grounds viz. Input voltage, PRF, Output voltage, Duration, Ringing, Devices employed and Mode of SRD. For better readability, the values of the comparison grounds corresponding to which our work has an edge over other reported works are highlighted in the table. In [47] results obtained are showing high ringing and the work does not seem to be cost effective as MESFET and amplifier are used in addition to SD and SRD. The work in [53] is having higher ringing as it uses SRD in shunt mode and the amplifier that has been employed [53], [56] is not a Pulsed-Power Amplifier (PPA) due to which nonlinearities are bound to creep in and the burnout probability is high on long term usage in pulsed mode of operation. Moreover, gain of the amplifier is frequency dependent over the concerned range of frequencies as confirmed from the specification sheet of the power amplifier (AM012535MM) used. In [60] the author employed an attenuator with relatively higher cost and the pulse duration obtained is also a concern.

Table 5.2: Comparison between Various Pulse Generators in Literature

Ref	Input voltage/PRF	Shape	Voltage (V)	Duration	Ringing in dB	Device	Mode
[47]	10 MHz	Monocycle	2	300ps	-14.5	SRD+SD+MESFET+Amplifier	Series
[48]	10 MHz	Monocycle	0.7	350ps	-20.9	SRD+SD(CPW)	Series
[49]	10 MHz	Monocycle	0.4	$\approx 300\text{ps}$	-17	SRD+2SDs	Series
[51]	3Vp-p/10 MHz	Pulse	1	300ps	-8.2		
		Pulse	1.3	600ps	-16.25		
		Pulse	1.6	1ns	-18.9	SRD+SD	Series
		Monocycle	1.65	1ns	-12.31		
[52]	7V pulses	Pulse	-2.5	140ps	-16	One SRD	
			-1.1	100ps	-14	2 SRDs	Shunt
[53]	3 Vp-p	Monocycle	15	400ps	-15.56	SRD+SD+Amplifier	Shunt
[56]	10 Vp-p/10 MHz	Pulse	5.6	241ps	-	2 SRDs + Amplifier	Shunt
[58]	20 Vp-p/12.2MHz	Pulse	6.2	166ps	-16	3 SRDs	Mixed
[60]	10Vp-p/10 kHz-10 MHz	Monocycle	1.80- 1.85	1ns	-17.15	SRD+SD +Attenuator	Series
[71]	12 MHz	Pulse	-6	$\approx 150\text{ps}$	-	SRD	Shunt
This work 4Vp-p/ 1MHz–100MHz		Pulse	0.87	170ps	-22		
		Monocycle	0.6	401ps	-16	SRD + SD	Series

Now, the comparative analysis is extended one more step by including the commercially available pulse generators at the Picosecond Pulse Labs [90]. A comprehensive comparison of the same is showcased in Table 5.3.

Table 5.3: Picosecond Pulse Labs Pulse generators [90]

Model	1000D	2600C		3500D	3600	4015D	4016	10050A	10060A	10070A	10300B	This work
Amplitude (V)	35	Turbo mode	Standard mode	> 8	7.5	1.9	2	10	10	7.5	+50 to +0.0045	0.87
		50	45								-45 to -0.004	
Waveform	Pulse	Pulse	Pulse	Pulse	Pulse	Step	Step	Pulse	Pulse	Pulse	Pulse	Pulse
Rise-time(ps)	250	250 (max. 350)	< 500	-	-	9	10	45	55	40 65	< 300	119
Fall-time(ps)	370	< 800 (max. 1800)	1000(max. 1800)	-	-	16	13	110	115	80	750	109
Pulse width(ps)	500(min 350 Max 600)	< 1000 to 10^5 (adjustable)		75 (max. 85)	70	22	18	$100 \text{ to } 10^4$	$100 \text{ to } 10^4$	$100 \text{ to } 10^4$	< 1ns to 100ns	170
Repetition rate	10Hz to 1MHz	1Hz to 100kHz		1Hz to 1MHz	< 100 Hz to 2.5 GHz	1Hz to 500 kHz	1Hz to 500kHz	1Hz to 100kHz	1Hz to 100kHz	1Hz to 100kHz	1Hz to 100kHz	1MHz to 100MHz
Jitter(ps)	< 7rms typical (12rms max.)	35 (RMS)	35 (RMS)	1.5 (RMS)	< 2 (RMS)	-	-	1.5	1.5	1.5	< 10 (rms)	1.58 (RMS) 10(Peak- Peak)
Polarity	Both	Either	Either	Either	Negative	Negative	Negative	Positive	Positive	Either	Either	Positive
Device/ Technology	Solid State	-	-	-	TTL gating function	-	-	Programmable IEEE-488	Programmable IEEE-488	Programmable IEEE-488	Programmable IEEE-488	SRD(no amplifier)

Chapter 6

Suitability to GPR

Preface

This chapter deals with the analysis of the aptness of the designed circuit for being used in GPR applications. Figures and tables are included to get a better understandability.

Ground Penetrating Radar (GPR) technology is among the fast maturing technologies in terms of theory and application. Over the past 15-20 years, it has grown into a major area of interest for researchers, engineers and industries. Reforms [46] made by regulatory bodies for electromagnetic spectrum usage across the globe have provided the necessary kicks and thrust for the growth of this technique. It has found its purpose in numerous fields like Glaciology, Geology, Hydrogeology, Archeology, Sedimentology and the like. A typical GPR configuration is shown in Figure 6.1 which gives a very basic idea of its working.

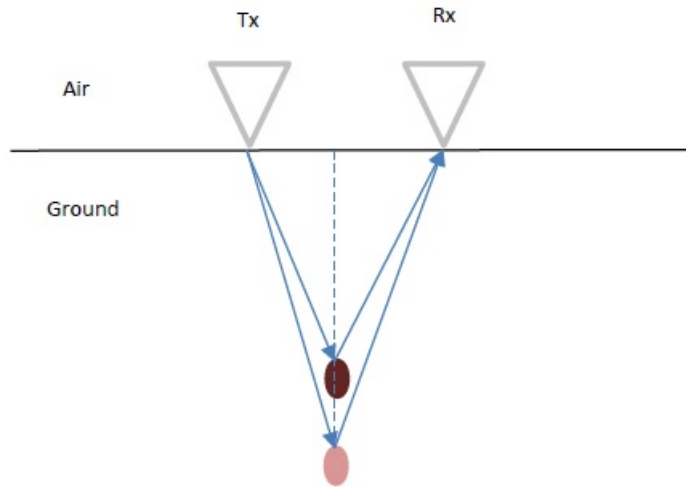


Figure 6.1: A typical GPR configuration

Depth resolution, which is one of the major performance evaluation parameters of a GPR device, is defined as the ability of the GPR device to distinguish between two layers of ground or objects beneath the ground having electrically different characteristics. The value of this parameter should be as low as possible (till the oscilloscope's sampling speed permits), so that it can detect finer changes in sub-surface electrical properties. The depth resolution corresponding to signals generated by different works are compared in a graphical manner in Figure 6.2. The plot shows depth resolution as a function of dielectric constant of the sub-surface medium. The dielectric constant dictates, velocity of wave in the medium. The wave velocity along with pulsewidth, according to (6.0.1), numerically decides the depth resolution (Δ_r) obtained, when the generated signal is shot vertically into the ground.

$$\Delta_r \geq \frac{T_{FWHM} * v}{4} \quad (6.0.1)$$

The above inequality gives the value of the best depth resolution for a temporal pulse having FWHM, T_{FWHM} and the sub-surface medium allowing wave velocity, v .

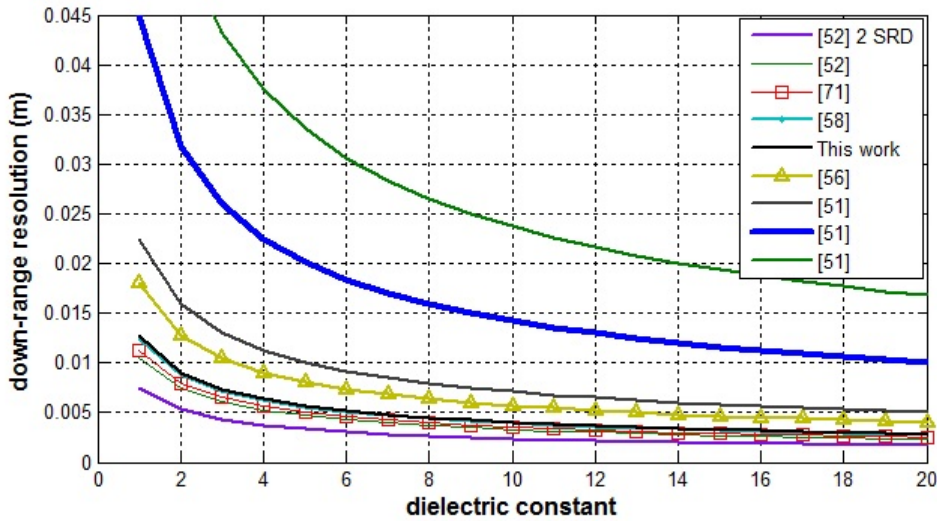


Figure 6.2: Resolution comparison of different reported works for Gaussian pulse

From the plot above, it can be concluded that, works in [52], [58], [71] are having numerically better depth resolution capability but as mentioned in Table 5.2, [52], [58] have a higher amount of ringing as compared to the work reported here due to the shunt mode of SRD. The ringing characteristic of [71] was not specified but as it also employs the SRD in shunt mode, it is highly likely to have a high ringing. The high amount of ringing will adversely affect the resolving capability of the above compared works when used in GPR applications.

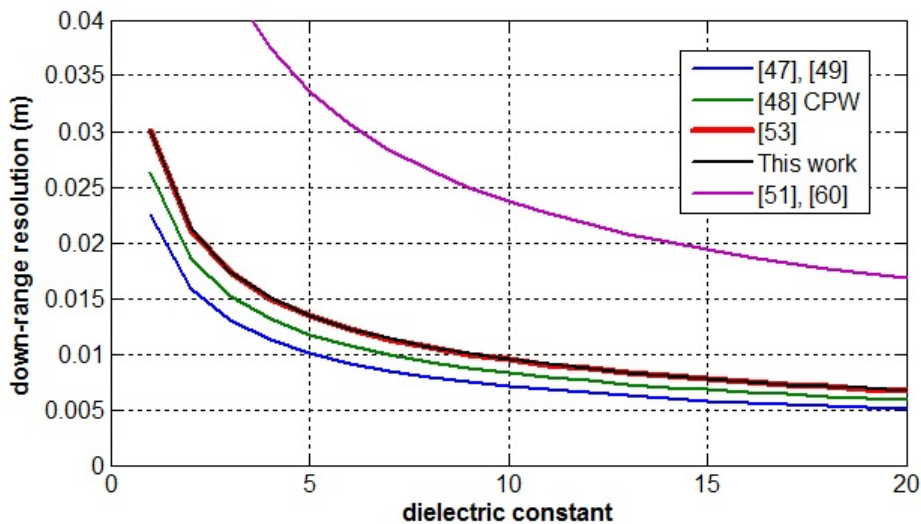


Figure 6.3: Resolution comparison of different reported works for Monocycle

The work [48] generating monocyte signal appears to be a good design but the major concern is the Co-planar Waveguide (CPW) technology that has been used. The CPWs have a low power handling capability and show higher radiation loss compared to the microstrip technology [88]. The works in [47], [49] show good prospect in GPR but [49] is having lower amplitude and the amplifier employed in [47] will demand high caution as a lot of heat will be generated on prolonged use, if proper heat sink is not provided. Now, another important parameter is peak power of the signal to be shot. The power requirement depends on factors like characteristic properties of the medium (attenuation constant, water content etc.), receiver sensitivity and penetration required. Generally, the power requirements are high due to the high attenuation in sub-surface wave propagation. The pulse generator designed in this work can be used in conjugation with a multi-stage Pulsed Power Amplifier (PPA) [91] employing the GaAs Heterojunction bipolar transistor. Amplification of the pulse can ease a considerable amount of pressure from the receiver sensitivity of the detector at the receiving end. Moreover, the PPAs show minor power dissipation as the transistors can be switched to cutoff mode when it is waiting for the next pulse to be amplified. Adverse effects of ringing tail can also be taken care of, by PPAs which would selectively amplify the pulse, discarding the ringing tail. In addition, PPAs have lesser chance of thermal instability as it gets some time to be cooled off and hence reduce nonlinearities to a large extent. The detection ability of the GPR device gets affected by radiations from the transmitting part in bistatic configuration. With regard to this issue, the circuit design technology that leads to least radiation should be implemented, like the Microstrip lines in comparison to CPWs. Moreover, GPR application needs the device to operate in high power ranges which is facilitated by microstrip lines in a better way than CPW [88]. The GPR device utilizing the reported pulse generator can also be mounted on a rover for covering a larger ground area. It will result into a large amount of data and the data analysis can also be done to capture the variation of the nature of soil in the area concerned if the PRF is low enough. A low PRF is required for GPR applications as it provides ample time for sampling and storage of the received data. Here, a PRF of 1MHz to 100MHz has been tested which is good for a pulse generator targeted for GPR applications.

Chapter 7

Conclusion and Scope for Future Work

Preface

In this final chapter, conclusions of the work carried out and suggested future scope for research work are presented.

7.1 Conclusions

Design, fabrication and analysis of temporal pulse generator circuits are presented in this thesis. The circuits have comparably remarkable characteristics like lower cost, lower ringing and negligible non-uniformity in delay. The circuits here are having better performance than the ones in literature and they also have potential to be more cost-effective and better in performance than some of the commercially available pulse generators. The fabricated circuits were also analyzed for jitter evaluation and showed a better performance than many of the commercially available pulse generators. Following are point-wise notable merits of the pulse generator circuits, designed and fabricated in the course of work for this thesis.

- The Gaussian pulse generator circuit design with good performance has been presented.
 - (a) The circuit is implemented in microstrip technology and has used low-cost lumped elements like resistors and capacitors. Also, the attenuator has been designed using resistive elements which has lowered the cost.
 - (b) The circuit has been found to be useful for low to medium range GPRs as the performance did not degrade for PRF from 1MHz to 100MHz.
 - (c) The circuit has proved to be a good high -speed circuit, as the random jitter was checked to be around 1.58ps (rms).
 - (d) The generated Gaussian pulse is having a very low ringing value of -22dB, a good bandwidth of 3.0GHz and low FWHM of 170ps which when used in GPR applications, can theoretically give a best resolution of 6.4mm for dry and sandy surface.
 - (e) The obtained signal has a better quality w.r.t. the ringing characteristic (-22dB) than most of the works in literature.
- The Monocycle pulse generator circuit with remarkable prospects in GPR has also been presented here.
 - (a) The circuit uses a differentiator rather than a shunt shorted stub to shape the Gaussian pulse into a Monocycle which results in a narrower pulsedwidth and a good symmetrical shape.
 - (b) The generated monocycle is having 162% fractional bandwidth which qualifies it to be a good quality UWB signal.
 - (c) The signal has an ultra-wide bandwidth of 4.3GHz which empowers it to be usable for heterogeneous mixtures of soil with different electrical characteristics.

7.2 Scope for Future Work

Presented below are the prospective research problems based on this work and possible improvements.

- In this work the microstrip based designs are presented whereas other planar structures like CPWs can be explored for improvements.
- Impedance matching of SRD with the rest of the circuit has been a challenge and the mismatches produce ringing in the circuit. These mismatches can be reduced further to avoid inclusion of the SD which can make the design more cost-effective.
- A PPA can be designed to amplify the signals generated by the circuits presented in this thesis. The amplified signal would make the whole circuit usable in GPR applications facilitating higher penetration.
- The established idea that odd order derivatives of the basic Gaussian pulse show better FCC spectral efficiency can be explored.

Appendix A

Matlab Codes for UWB waveforms

A.1 Family of Gaussian pulse

```
clear all;
Fs=100E9; %sampling frequency
ts = 1/Fs;
t = -1e-9:ts:1e-9;
t1 = 200e-12; %pulsewidth
```

A.1.1 Basic Gaussian pulse

```
%gaussian pulse
g = exp(-0.5*((t-(t1/2))/(t1/7)).*((t-(t1/2))/(t1/7)));
figure(1);
plot(t,g); grid on;
l = size(t); L = l(1,2);
NFFT = 2^nextpow2(L);
G = fft(g,NFFT)/L;
f = Fs/2*linspace(0,1,NFFT/2+1);
% Plot single-sided amplitude spectrum.
figure(2);
plot(f,2*abs(G(1:NFFT/2+1)));
grid on;
title('Spectrum of g(t)');
xlabel('Frequency (Hz)');
ylabel('|G(f)|');
```

The basic Gaussian pulse is shown in Figure B.1 along with its spectrum in Figure B.2.

A.1.2 Monocycle pulse

```
%corresponding Monocycle pulse by
%differentiating the gaussian pulse
m=-49*((t-t1/2)/(t1^2)).*g;
figure(3);
plot(t,m);
grid on;
title('Monocycle pulse signal');
xlabel('time (sec)');
ylabel('m(t)');
M = fft(m,NFFT)/L;
figure(4);
plot(f,2*abs(M(1:NFFT/2+1)));
grid on;
title('Spectrum of m(t)');
xlabel('Frequency (Hz)');
ylabel('|M(f)|');
```

The Monocycle pulse is shown in Figure B.3 along with its spectrum in Figure B.4.

A.1.3 Mexican Hat pulse

```
%corresponding Mexican Hat pulse by
%differentiating the Monocycle pulse
mh=(-49/(t1^2)+(2401*((t-(t1/2))/(t1^2)).^2)).*g;
figure(5);
plot(t,mh);
grid on;
title('Mexican Hat pulse signal');
xlabel('time (sec)');
ylabel('mh(t)');
MH = fft(mh,NFFT)/L;
figure(6);
plot(f,2*abs(MH(1:NFFT/2+1)));
grid on;
title('Spectrum of mh(t)');
xlabel('Frequency (Hz)');
ylabel('|MH(f)|');
```

The Mexican Hat pulse is shown in Figure B.5 along with its spectrum in Figure B.6.

A.2 Orthogonal Modified Hermite pulse family

```
Fs=1e10; %sampling frequency
ts = 1/Fs;
t = 5*(-1e-9):ts:5*(1e-9);
t1 = 170E-12; %pulsewidth
```

A.2.1 Zeroth order OMHP

```
%zeroth order OMHP
h0 = exp(-0.25*((t/(2*t1)).*(t/(2*t1)))); %Zeroth order OMHP
figure(7);
plot(t,h0); grid on;
l = size(t); L = l(1,2);
NFFT = 2^nextpow2(L);
H0 = fft(h0,NFFT)/L;
f = Fs/2*linspace(0,1,NFFT/2+1);
% Plot amplitude spectrum.
figure(8);
plot(f,2*abs(H0(1:NFFT/2+1)));
grid on;
title('Spectrum of h0(t)');
xlabel('Frequency (Hz)');
ylabel('|H0(f)|');
```

The Zeroth order OMHP is shown in Figure B.7 along with its spectrum in Figure B.8.

A.2.2 First Order OMHP

```
%First order OMHP
h1=(t/t1).*h0;
figure(9);
plot(t,h1);
grid on;
title('OMHP class order 1 pulse');
xlabel('time (sec)');
ylabel('h1(t)');
H1 = fft(h1,NFFT)/L;
figure(10);
plot(f,2*abs(H1(1:NFFT/2+1)));
grid on;
```

```

title('Spectrum of h1(t)');
xlabel('Frequency (Hz)');
ylabel('|H1(f)|');

```

The First order OMHP is shown in Figure B.9 along with its spectrum in Figure B.10.

A.2.3 Second Order OMHP

```

%Second order OMHP
h2=(((t/t1).^2)-1).*h0;
figure(11);
plot(t,h2);
grid on;
title('OMHP class order 2 pulse');
xlabel('time (sec)');
ylabel('h2(t)');
H2 = fft(h2,NFFT)/L;
figure(12);
plot(f,2*abs(H2(1:NFFT/2+1)));
grid on;
title('Spectrum of h2(t)');
xlabel('Frequency (Hz)');
ylabel('|H2(f)|');

```

The Second order OMHP is shown in Figure B.11 along with its spectrum in Figure B.12.

A.3 Prolate Spheroidal pulse family

```

Fs=50*1e9; %sampling frequency
ts = 1/Fs;
fU=10.6*1e9;
fL=3.1*1e9;
fC=(fU+fL)/2;
t = -(1e-9):ts:(1e-9);
t1 = 170e-12; %pulsewidth
c=t1*2*pi*(fU-fL)/2;
%approximate Prolate spheroidal pulse
apsp = (sin(c*sqrt(((t-(t1/2))/t1).^2)-1))./
(sinh(c)*sqrt(((t-(t1/2))/t1).^2)-1));

```

```
figure(13);
plot(t,apsp); grid on;
title('APSP');
xlabel('time (sec)');
ylabel('apsp(t)');
l = size(t); L = l(1,2);
NFFT = 2^nextpow2(L);
APSP = fft(apsp,NFFT)/L;
f = Fs/2*linspace (0,1,NFFT/2+1);
% Plot amplitude spectrum.
figure(14);
plot(f,2*abs(APSP(1:NFFT/2+1)));
grid on;
title('Spectrum of apsp(t)');
xlabel('Frequency (Hz)');
ylabel('|APSP(f)|');
```

The Approximate Prolate Spheroidal pulse is shown in Figure B.13 along with its spectrum in Figure B.14.

Appendix B

Plots of UWB waveforms

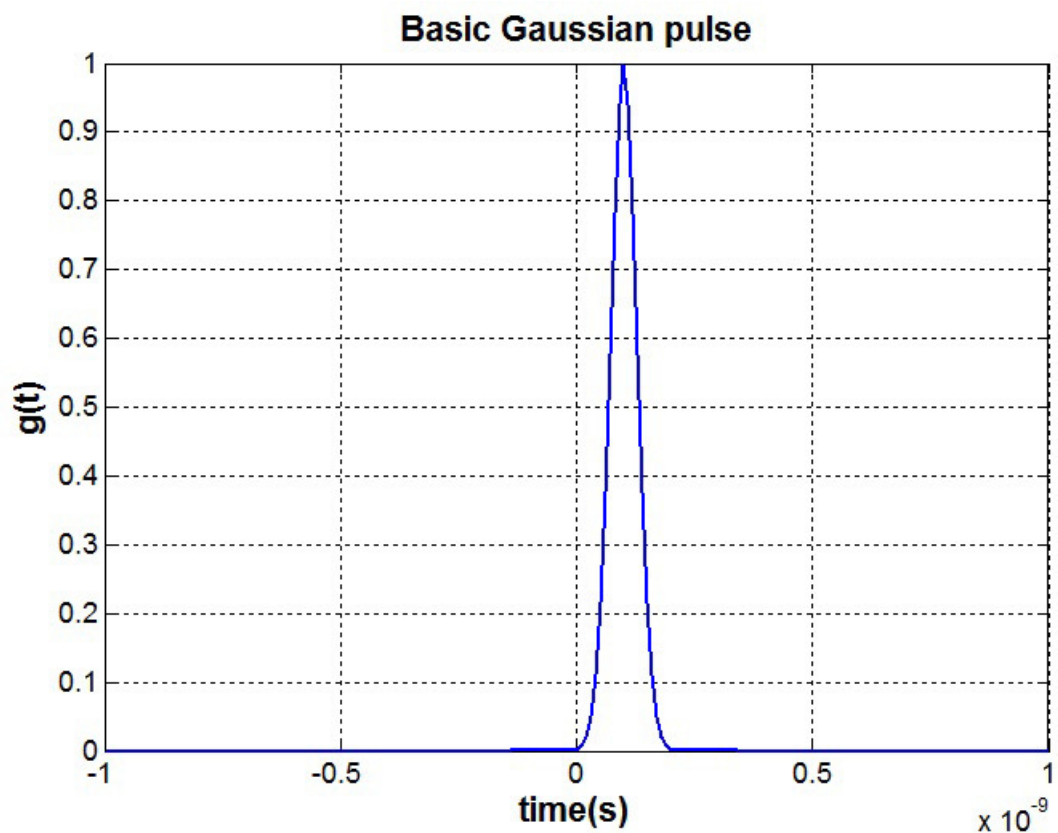


Figure B.1: Gaussian pulse (time domain)

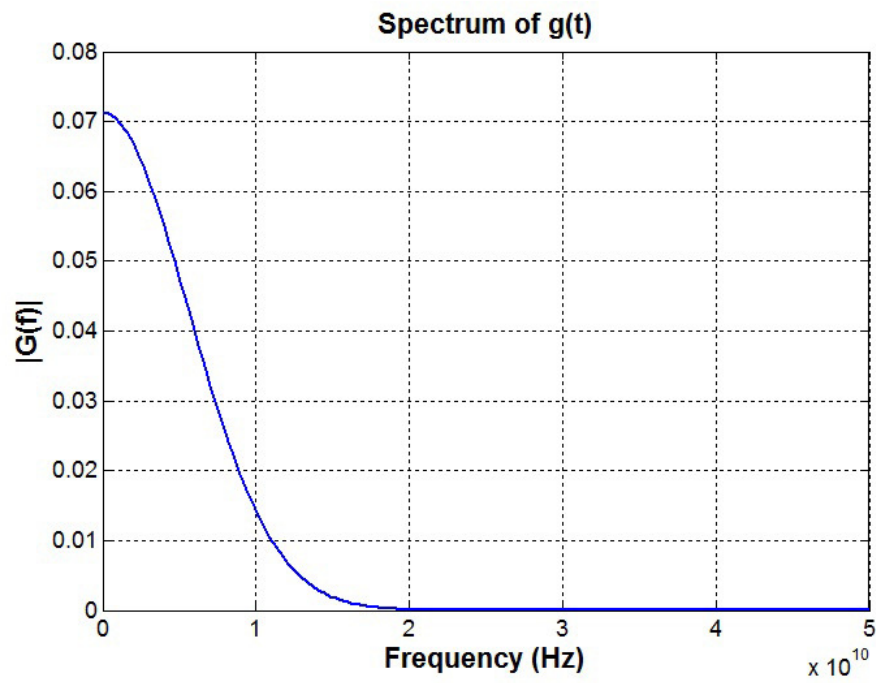


Figure B.2: Spectrum of the Gaussian pulse

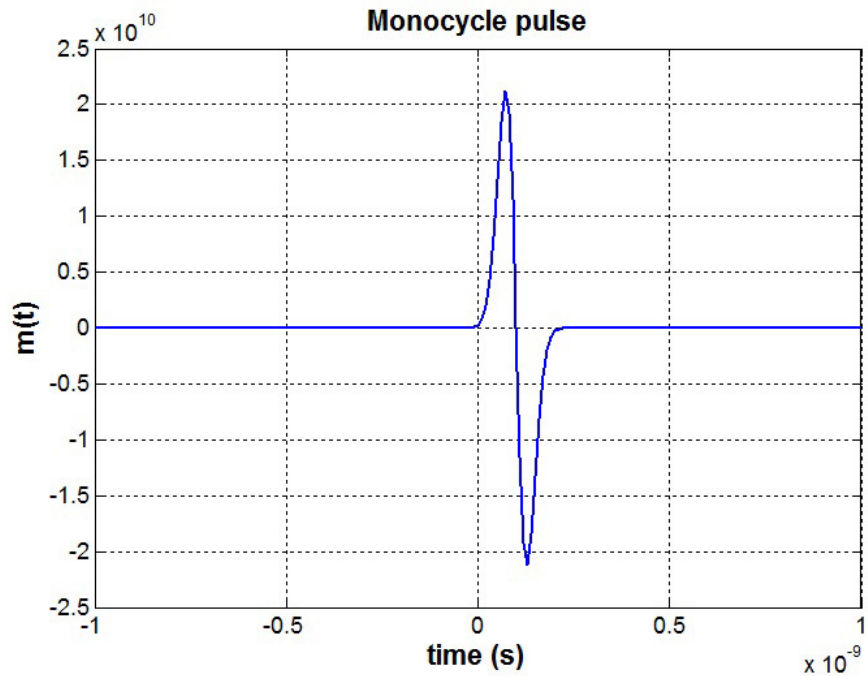


Figure B.3: Monocycle pulse (time domain)

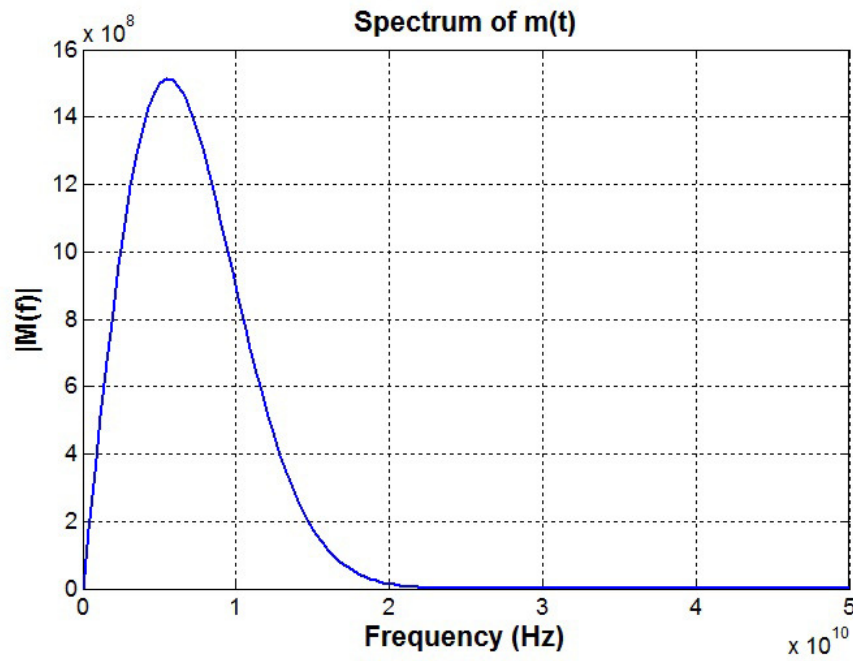


Figure B.4: Spectrum of the monocycle pulse

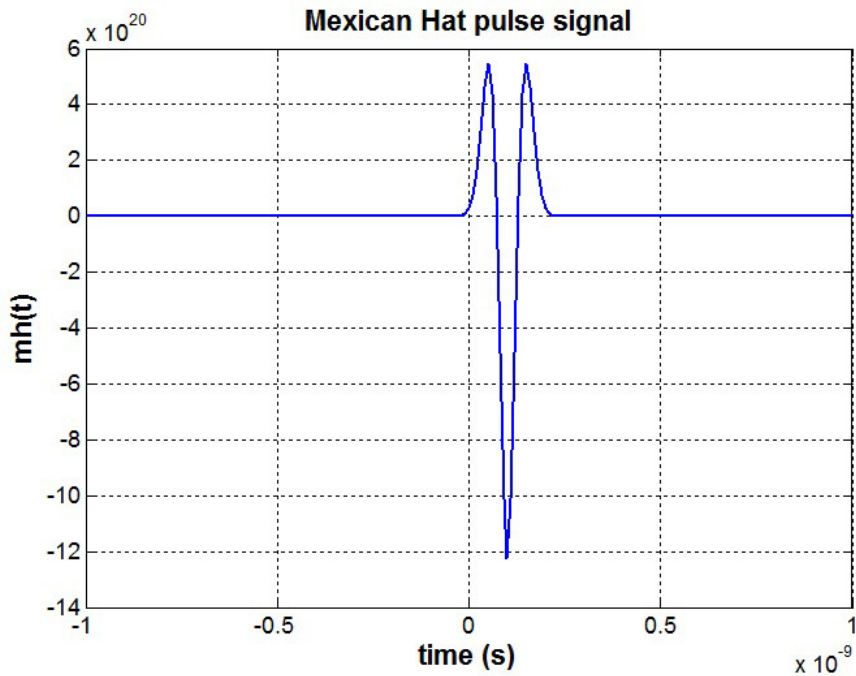


Figure B.5: Mexican Hat pulse (time domain)

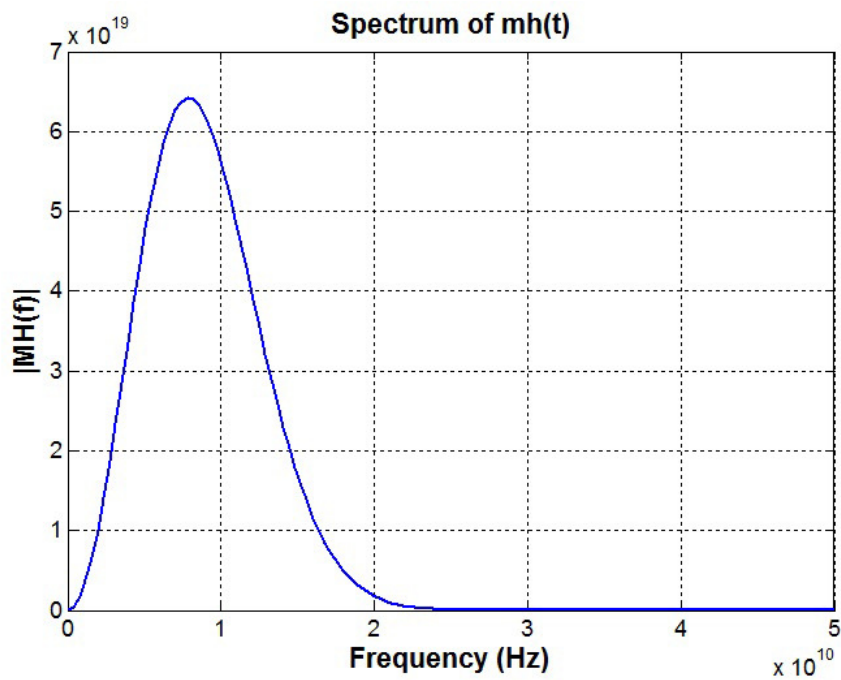


Figure B.6: Spectrum of the Mexican Hat Pulse

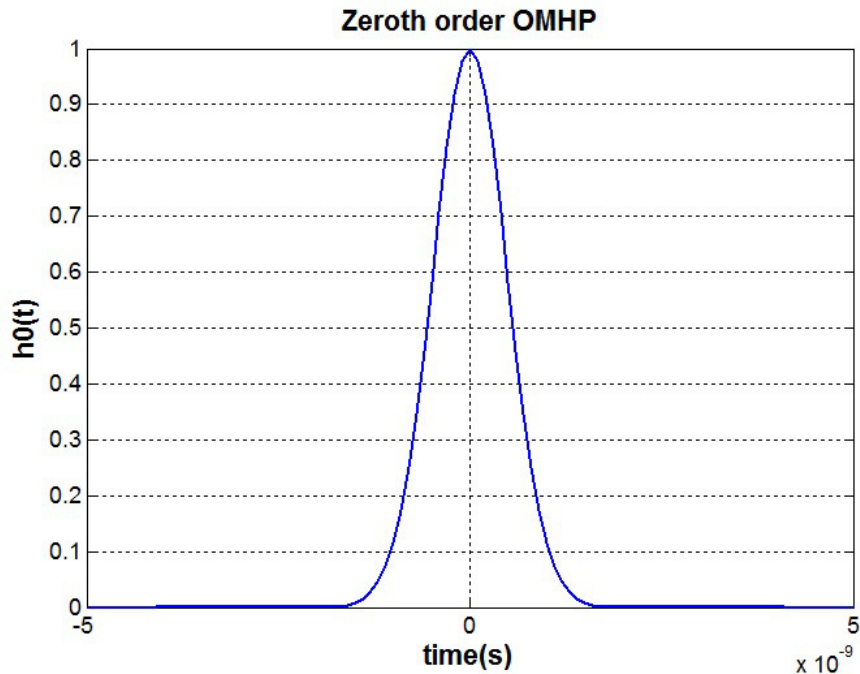


Figure B.7: OMHP 0th order signal

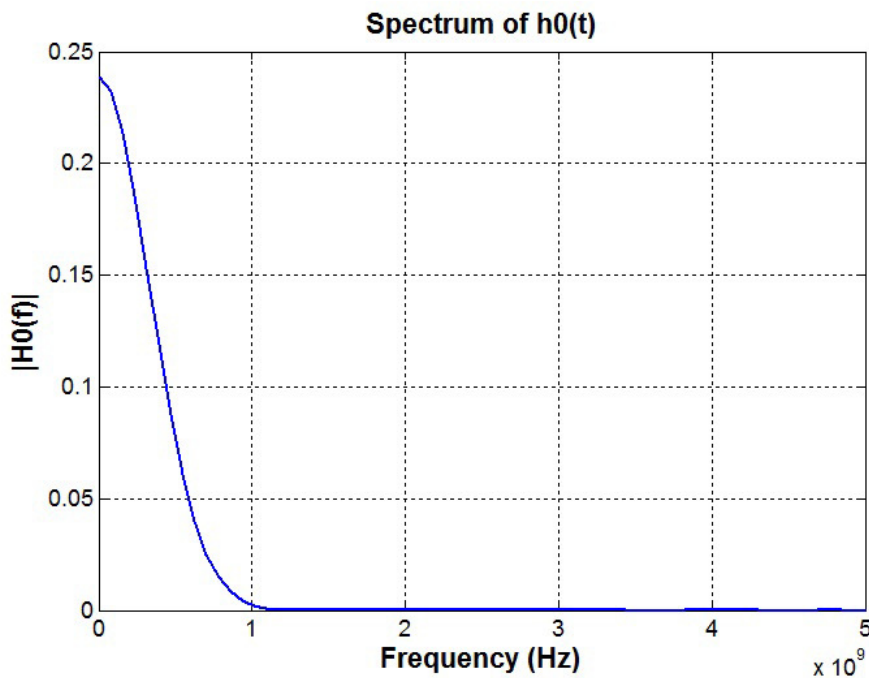


Figure B.8: Spectrum of OMHP 0th order signal

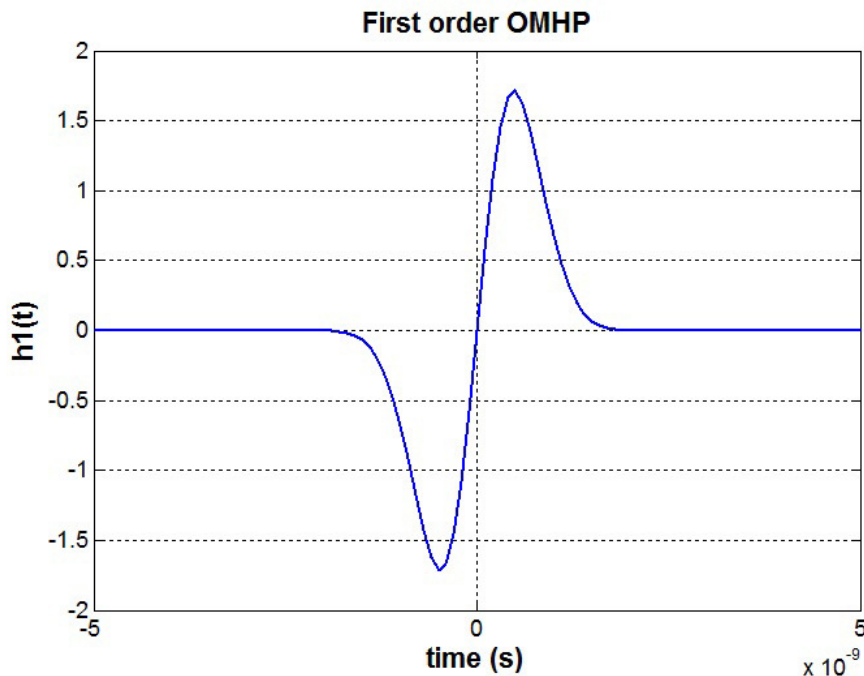


Figure B.9: OMHP 1st order signal

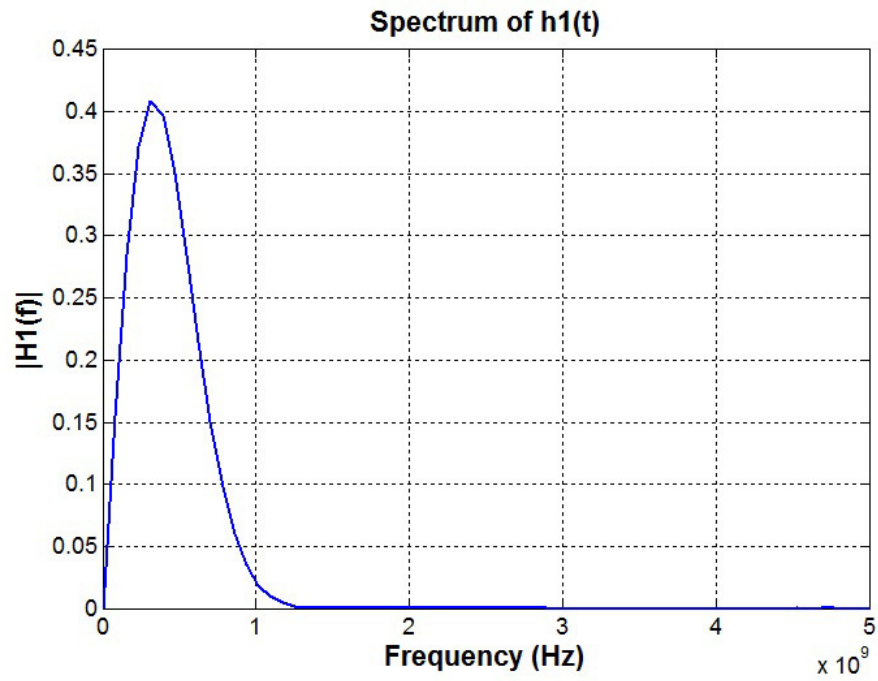


Figure B.10: Spectrum of OMHP 1st order signal

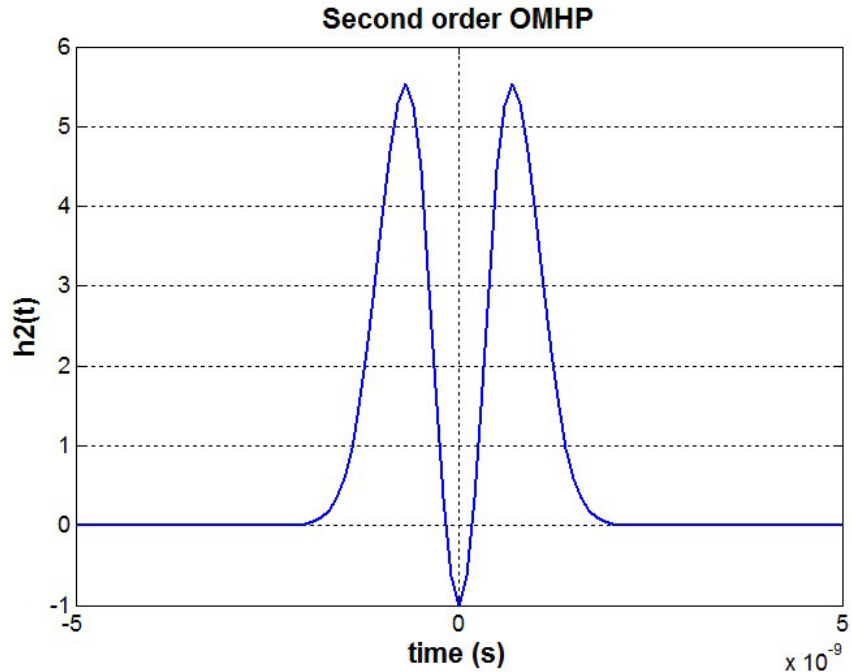


Figure B.11: OMHP 2nd order signal

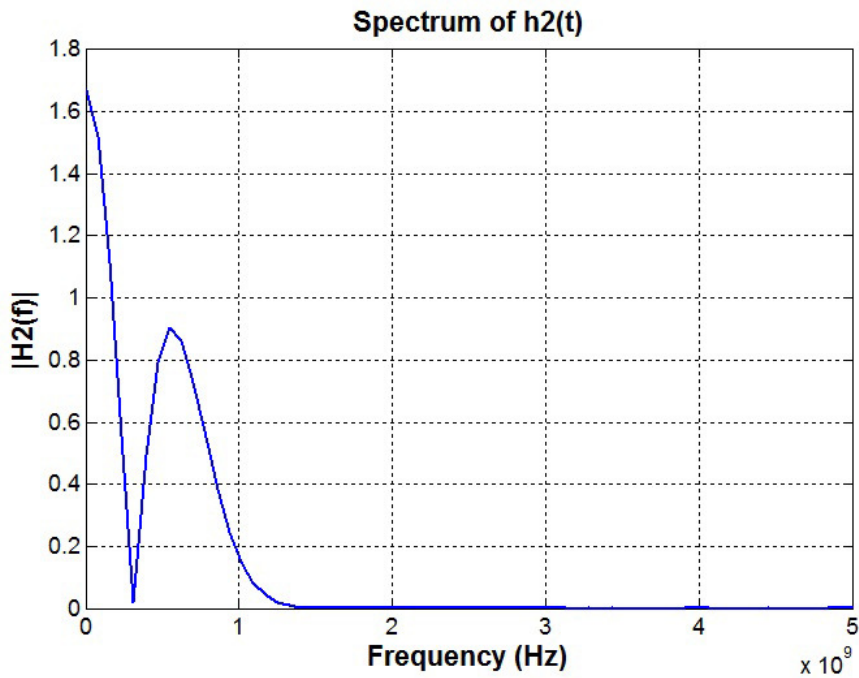


Figure B.12: Spectrum of OMHP 2nd order signal

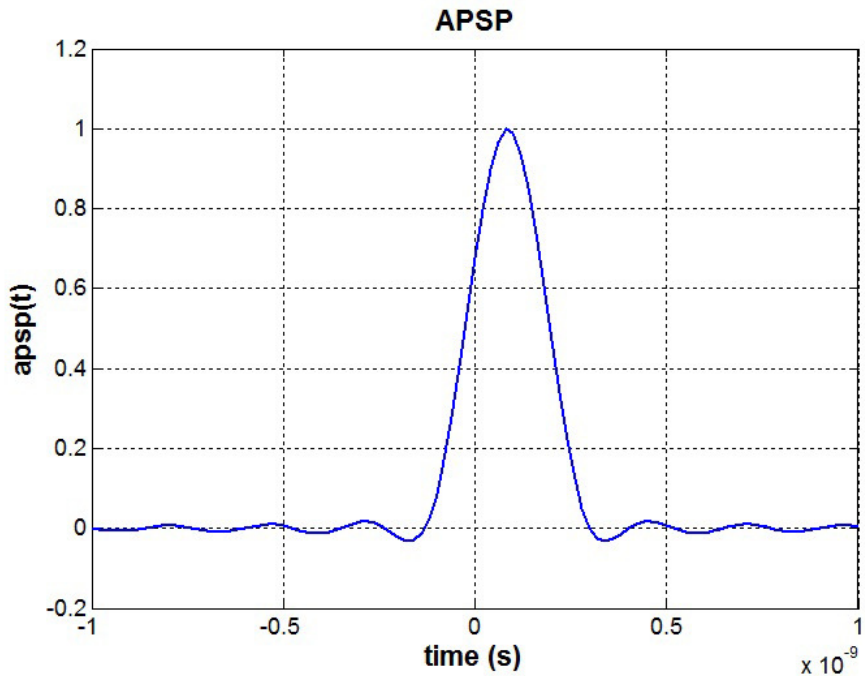


Figure B.13: APSP Signal

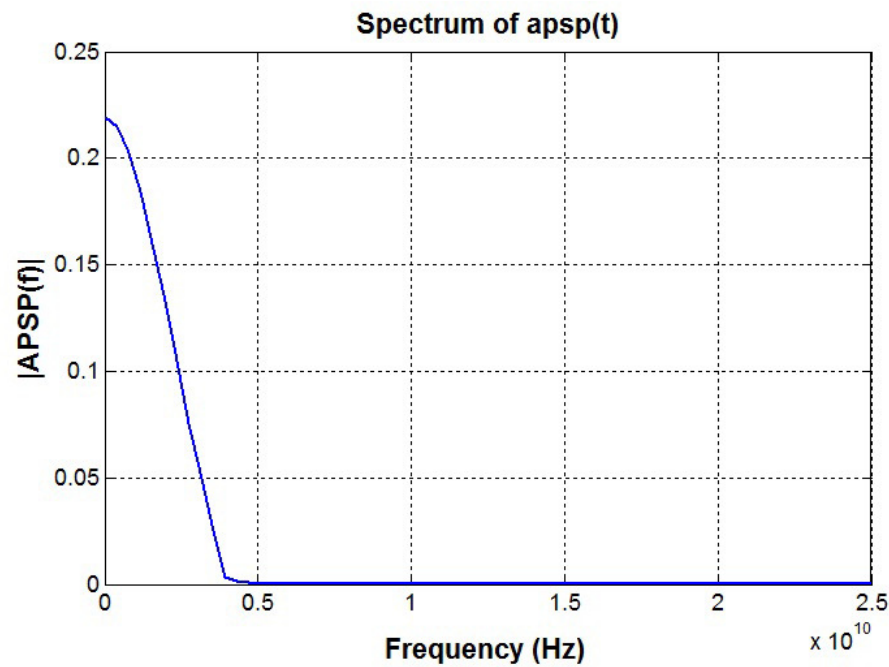


Figure B.14: Spectrum of APSP signal

References

- [1] R. H. Kingston, "Switching time in junction diodes and junction transistors," *Proc. of IRE*, May 1954.
- [2] B. Lax and S. F. Neustadter, "Transient response of a pn junction," *Journal of Applied Physics*, vol. 25, no. 9, Sep. 1954.
- [3] J. M. A. F. Boff and R. Shen, "A new high-speed effect in solid-state diodes," *Proc. IEEE Int. Solid-State Circuits Conf. Dig. Tech. Papers*, vol. 3, 1960.
- [4] S. K. J. L. Moll and R. Shen, "P-n junction charge-storage diodes," *Proc. of the IRE*, Jan. 1962.
- [5] S. M. Krakauer, "Harmonic generation, rectification, and lifetime evaluation with the step recovery diode," *Proc. of the IRE*, Jul. 1962.
- [6] B. L. Diamond, "Idler circuits in varactor frequency multipliers," *IEEE Trans. on Circuit Theory*, Mar. 1963.
- [7] K. Husimi and T. Inamura, "Pulse-time modulation and frequency modulation using the step recovery diode," *Proc. of the IEEE*, Jan. 1964.
- [8] R. B. Mouw and F. S. Coale, "Microwave applications of the step recovery diode," *PTGMMT International Symposium Digest*, 1964, vol. 64, no. 1b, 1964.
- [9] J. Chernak and C. F. Simone, "Simple equivalent circuits for a step recovery diode and a switching transistor," *IEEE Trans. on Electronic Computers*, Oct. 1964.
- [10] R. D. Hall, "Frequency multiplication with the step recovery diode," *G-MTT Symposium Digest 1965*, vol. 65, no. 1,
- [11] K. L. Kotzebue, "A circuit model of the step recovery diode," *Proc. IEEE*, Dec. 1965.
- [12] J. R. A. D. E. Crane J. W. Baitles, "A hysteresis effect in step recovery millimeter wave harmonic generators," *IEEE Proc. Letters*, Dec. 1966.
- [13] J. C. Mcdade, "Measurement of additive phase noise contributed by the step-recovery diode in a frequency multiplier," *Proc. of the IEEE*, Feb. 1966.

- [14] R. Thompson, "Step-recovery-diode frequency multiplier," *IEEE Electron Letters*, vol. 2, no. 3, Mar. 1966.
- [15] S. H. Izadpanah and I. M. Stephenson, "Circuit arrangements for step recovery diode multipliers," *Proc. of the IEEE*, Mar. 1967.
- [16] H. Benda and E. Spenke, "Reverse recovery process in silicon power rectifiers," *Proc. IEEE*, vol. 55, no. 8, Aug. 1967.
- [17] H. T. Friis, "Analysis of harmonic generator circuits for step recovery diodes," *Proc. of the IEEE*, vol. 55, no. 7, Jul. 1967.
- [18] S. V. Judd, "High-order multipliers without idlers," *Radio and Electronic Engineer*, vol. 34, no. 1, Jul. 1967.
- [19] J. G. Gardiner, "The step-recovery diode in harmonic generation: a linear time-varying circuit model," *Radio and Electronic Engineer*, vol. 34, no. 3, Sep. 1967.
- [20] W. M. V. Loock, "Working conditions of a step-recovery diode multiplier allowing one conduction angle per cycle," *Proc. Letters*, 1968.
- [21] ——, "Conditions for single conduction in a series-type frequency multiplier using an ideal step-recovery diode," *Electronics Letters*, vol. 5,
- [22] P. W. Chivlers, "Generalised efficiency curve for step-recovery-diode frequency multipliers," *Electronic Letters*, vol. 4, no. 22, Nov. 1968.
- [23] W. M. V. Loock and A. Cardon, "Theoretical analysis of ideal step-recovery diode in series-mode operation," *Radio and Electronic Engineer*, May 1968.
- [24] P. W. Chivlers, "Modified circuit model for the step-recovery diode to include nonzero transition time," *Electronics Letters*, vol. 5, no. 15, Jul. 1969.
- [25] J. L. Moll and S. A. Hamilton, "Physical modeling of the pulse and harmonic step recovery diode for generation circuits," *Proc. of the IEEE*, vol. 57, no. 7, Jul. 1969.
- [26] R. H. Dean and C. J. Nuese, "A refined step-recovery technique for measuring minority carrier lifetimes and related parameters in asymmetric p-n junction diodes," *IEEE Trans. on Electron Devices*, vol. ED-18, no. 3, Mar. 1971.
- [27] P. E. Gibbons, "Problems concerning the spatial distribution of deep impurities in semiconductors," *Solid-State Electronics*, vol. 12, no. 12, Dec. 1969.
- [28] R. J. Chaffin, "Neutron damage effects in step recovery diode frequency multipliers," *IEEE Trans. on Nuclear Science*, vol. 18, no. 6, 1971.
- [29] M. Karadeniz, "New subnanosecond pulse-generator circuit employing two step-recovery diodes," *Electronics Letters*, vol. 10, no. 7, Apr. 1974.
- [30] J. M. Coles and R. J. Smith-Saville, "High-repetition-rate step-recovery-diode monostable circuits," *Electronics Letters*, vol. 10, no. 20, Oct. 1974.

- [31] P. L. Ntake and D. R. Conn, "Frequency multiplication by a p-i-n diode driven into avalanche breakdown," *IEEE Trans. on Microwave Theory and Techniques*, Jun. 1975.
- [32] H. M. Cronson, "Picosecond-pulse sequential waveform generation," *IEEE Trans. on Microwave Theory and Techniques*, Dec. 1975.
- [33] R. Tielert, "Subnanosecond-pulse generator employing 2-stage pulse step sharpener," *Electronics Letters*, vol. 12, no. 3, Feb. 1976.
- [34] H. M. C. A. Murray Nicolson and P. G. Mitchell, "Subnanosecond risetime pulse generators," *IEEE Trans. on Instrumentation and Measurement*, vol. 25, no. 2, Jun. 1976.
- [35] H. M. Masayoshi Naito and T. Ogawa, "High current characteristics of asymmetrical p-i-n diodes having low forward voltage drops," *IEEE Trans. on Electron Devices*, vol. Ed-23, no. 8, Aug. 1976.
- [36] R. Tielert and B. G. Bosch, "An improved circuit model of the step-recovery diode for computer-aided design," *IEEE Periodical*, vol. 22, 1976.
- [37] D. M. Delauder and C. M. Balanis, "Microwave short-pulse generator for bed-level detection," *IEEE Trans. on Instrumentation and Measurement*, vol. IM-31, no. 4, Dec. 1982.
- [38] T. G. N. J. Rudie J. Wilkenfeld and J. Rutherford, "Pulsed power burnout testing of microwave diodes," *IEEE Trans. on Nuclear Science*, vol. NS-32, no. 6, Dec. 1985.
- [39] D. E. M. M. R. T. Tan S. T. Wang and J. L. Moll, "12ps gaas double heterostructure step recovery diode," *Electronics Letters*, vol. 28, no. 7, Mar. 1992.
- [40] M. T. Sameer P. Pendharkar and K. Shenai, "Dynamics of reverse recovery of high power p-i-n diodes," *IEEE Trans. on Electron Devices*, vol. 43, no. 1, Jan. 1996.
- [41] F.-Y. Chang, "Transient analysis of diode switching circuits including charge storage effect," *IEEE Trans. on Circuits and Systems-I: Fundamental Theory and Applications*, vol. 43, no. 3, Mar. 1996.
- [42] E. S. R. J. Focia and C. B. Fleddermann, "Simple techniques for the generation of high peak power pulses with nanosecond and subnanosecond rise times," *Rev. Sci. Instrum.*, vol. 67, no. 7, Jul. 1996.
- [43] J. Zhang and A. V. Raisanen, "Computer-aided design of step recovery diode frequency multiplier," *IEEE Trans. on Microwave Theory and Techniques*, vol. 44, no. 12, Dec. 1996.

- [44] M. J. Chudobiak and D. J. Walkey, "Forward transient charge injection in psn diodes at medium to high injection levels," *IEEE Trans. on Electron Devices*, vol. 44, no. 1, Jan. 1997.
- [45] K. S. D. V. M. Jenett V. Naumenko and V. Volkov, "2kv generator for subnanosecond pulses," *Electronics Letters*, vol. 33, no. 11, May 1997.
- [46] F. C. Commission, "Revision of part 15 of the commission's rules regarding ultra-wideband transmission systems," first report and order, fcc 02.v48," Apr. 2002.
- [47] J. S. Lee and C. Nguyen, "Novel low-cost ultra-wideband, ultra-short-pulse transmitter with mesfet impulse-shaping circuitry for reduced distortion and improved pulse repetition rate," *IEEE Microwave and Wireless Components Letters*, vol. 11, no. 5, May 2001.
- [48] C. N. Jeong Soo Lee and T. Scullion, "New uniplanar subnanosecond monocycle pulse generator and transformer for time-domain microwave applications," *IEEE Trans. on Microwave Theory and Techniques*, vol. 49, no. 6, Jun. 2001.
- [49] J. Han and C. Nguyen, "A new ultra-wideband, ultra-short monocycle pulse generator with reduced ringing," *IEEE Microwave and Wireless Components Letters*, vol. 12, no. 6, Jun. 2002.
- [50] ———, "Ultra-wideband electronically tunable pulse generators," *IEEE Microwave and Wireless Components Letters*, vol. 14, no. 3, Mar. 2004.
- [51] C. Zhang and A. E. Fathy, "Reconfigurable pico-pulse generator for uwb application," *2006 IEEE MTT-S Int. Microwave Symposium Digest*, Jun. 2006.
- [52] J. W. Amnoiy Ruengwaree Abhijit Ghose and G. Kompa, "Ultra-fast pulse transmitter for uwb microwave radar," *Proceedings of the 36th European Microwave Conference*, 2006.
- [53] X. G. J. Zhou and Y. Fei, "A new cad model of step recovery diode and generation of uwb signals," *IEICE Electron. Exp.*, vol. 3, no. 24, Dec. 2006.
- [54] P.-K. C. T.-G. Ma C.-J. Wu and C.-F. Chou, "Ultrawideband monocycle pulse generator with dual resistive loaded shunt stubs," *Microw. Opt. Technol. Lett.*, vol. 49, no. 2, Feb. 2007.
- [55] A. N. F. A. P. D. S. Lev M. Merensky Alexei F. Kardo-Sysoev and A. S. Kesar, "A low-jitter 1.8-kv 100-ps rise-time 50-khz repetition-rate pulsed-power generator," *IEEE Trans. on Plasma Science*, vol. 37, no. 9, Sep. 2009.
- [56] A.-C. T. K.K.-M. Chan K. Rambabu and M.-W. Chia, "Efficient passive low-rate pulse generator for ultra-wideband radar," *IET Microw. Antennas Propag.*, vol. 4, no. 12, 2010.

- [57] L. Liu and G. Fang, "A novel uwb sampling receiver and its applications for impulse gpr systems," *IEEE Geoscience and Remote Sensing Letters*, vol. 7, no. 4, Oct. 2010.
- [58] J. J. C. Gil Wong Choi and S. H. Han, "Picosecond impulse generator driven by cascaded step recovery diode pulse shaping circuit," *Rev. Sci. Instrum.*, vol. 82, 016106, Jan. 2011.
- [59] H. W.-Z. L. Xiudong Yang Yongdong Li and Z. Ding, "Numerical investigation of the nanosecond opening-mechanism of drift step recovery diodes," *Journal of Applied Physics*, vol. 109, 014917, Jan. 2011.
- [60] A. S. V. Tian Xia and H. Dryver, "A high-performance low-ringing ultrawideband monocycle pulse generator," *IEEE Trans. on Instrumentation and Measurement*, vol. 61, no. 1, 2012.
- [61] L. M. M. I. S. Amit S. Kesar Yaakov Sharabani and A. Sher, "Drift-step-recovery diode characterization by a bipolar pulsed power circuit," *IEEE Trans. on Plasma Science*, vol. 40, no. 11, Nov. 2012.
- [62] H. G. Xinfan Xia Lihua Liu and G. Fang, "Balanced pulse generator for uwb radar application," *Electronics Letters*, vol. 49, no. 4, Feb. 2013.
- [63] M. R. D. B. A. Benedetto F. Benedetto and G. Giunta, "Reliability of signal processing technique for pavement damages detection and classification using ground penetrating radar," *IEEE Sensors J.*, vol. 5, no. 3, Jun. 2005.
- [64] S. M. Salvador and G. Vecchi, "On some experiments with uwb microwave imaging for breast cancer detection," *Proc. IEEE AP-S Int. Symp.*, Jun. 2007.
- [65] A. M. A. De Angelis M. Dionigi and P. Carbone, "A low-cost ultra-wideband indoor ranging system," *IEEE Trans. Instrumen. Meas.*, vol. 58, no. 12, Dec. 2009.
- [66] P. M. N. Maaref and X. Ferri'eres, "Electromagnetic imaging method based on time reversal processing applied to through-the-wall target localization," *Progress In Electromagnetics Research M*, vol. 1, 2008.
- [67] Y. Q. Yang and A. E. Fathy, "Development and implementation of a realtime see-through-wall radar system based on fpga," *IEEE Trans. Geosci. Remote Sens.*, vol. 47, no. 5, May 2009.
- [68] E. S. H. S. L. Earp, T. J. Elkins, and R. Vickers, "Ultra-wideband ground-penetrating radar detection of buried metallic mines," *IEEE AES Systems Magazine*, Sep. 1996.
- [69] W. W. O. Hirsch M. Janson and R. S. Thoma, "Indirect localization and imaging of objects in an uwb sensor network," *IEEE Trans. Instrumen. Meas.*, vol. 59, no. 11, Nov. 2010.

- [70] Y.-L. Y. Chin-Lung Yang and C.-C. Lo, "Subnanosecond pulse generators for impulsive wireless power transmission and reception," *IEEE Trans. on Circuits and Systems—II: Express Briefs*, vol. 58, no. 12, Dec. 2011.
- [71] J. Han and C. Nguyen, "Coupled-slotline-hybrid sampling mixer integrated with step-recovery-diode pulse generator for uwb applications," *IEEE Trans. Microwave Theory and Techniques*, vol. 53, no. 6, Jun. 2005.
- [72] C. J. W. T. G. Ma and C. Chou, "An impulse-radio-based ultrawideband rf front-end module with a new multilayered microwave sampler," *Progress In Electromagnetics Research Letters*, vol. 86, 2008.
- [73] S. Mizushina, "Triggered operation of tunnel diode oscillators and pulse generators," *IEEE Journal of Solid-State Circuits*, vol. SC-2, no. 3, Sep. 1967.
- [74] Z. C. Tan, "Tunnel diode narrow pulse generator," *Proc. Letters of IEEE*, Nov. 1973.
- [75] K. M. M. M. Dongpo Wu Jie Pan and K. Maezawa, "Ultrashort pulse generators using resonant tunneling diodes with improved power performance," *The 25th International Conference on Indium Phosphide and Related Materials*, May 2013.
- [76] M. Bramson, "Application of avalanche transistors to 10-megacycle pulse generators," *IRE Trans. on Nuclear Science*, vol. 9, no. 4, Aug. 1962.
- [77] H. M. Rein and M. Zahn, "Subnanosecond-pulse generator with variable pulselwidth using avalanche transistors," *Electronics Letters*, vol. 11, no. 1, Jan. 1975.
- [78] P. T. V. Pavitra Krishnaswamy Andras Kuthi and M. A. Gundersen, "Compact subnanosecond pulse generator using avalanche transistors for cell electroperturbation studies," *IEEE Trans. on Dielectrics and Electrical Insulation*, vol. 14, no. 4, Aug. 2007.
- [79] D. P. F. Zito and D. Zito, "Uwb cmos monocycle pulse generator," *IEEE Trans. Circuits Syst. I*, vol. 57, no. 10, Oct. 2010.
- [80] O. Lemaire and T. Xia, "Design of a monolithic width programmable gaussian monocycle pulse generator for ultra wideband radar in cmos technology," *Proc. Joint IEEE NEWCAS TAISA Conf.*, Jun. 2009.
- [81] N. S. T. Kikkawa P. K. Saha and K. Kimoto, "Gaussian monocycle pulse transmitter using 0.18 m cmos technology with on-chip integrated antennas for inter-chip uwb communication," *IEEE J. Solid-State Circuits*, vol. 43, no. 5, May 2008.
- [82] J. M. Pavel Protiva and J. Machac, "A compact step recovery diode subnanosecond pulse generator," *Microwave and Optical Technology Letters*, vol. 52, no. 2, Feb. 2010.

- [83] A. A. Mohammad Ghavami and F. Marvasti, "Unified structure of basic uwb waveforms," *IEEE Trans. on Circuits and Systems—II: Express Briefs*, vol. 55, no. 12, Dec. 2008.
- [84] L. Yin and Z. Hongbo, "Uwb pulse design using the approximate prolate spheroidal wave functions," *2005 IEEE International Symposium on Microwave, Antenna, Propagation and EMC Technologies for Wireless Communications Proceedings*, 2005.
- [85] Y. Guo, "Optimal waveform design for ultra-wideband communication based on gaussian derivatives," *Journal of Communications and Networks*, vol. 10, no. 4, Dec. 2008.
- [86] C. T. Y. E. F. B. L. Sakkila A. Rivenq and J. M. Rouvaen, "Comparison of classical and orthogonal uwb waveforms for radar applications," *6th International Colloquium on Signal Processing and Its Applications (CSPA)*, 2010.
- [87] K. Li, "Experimental study on uwb pulse generation using uwb band pass filters," *Proc. Of IEEE Conf. on Ultra Wideband*, vol. 4, 2006.
- [88] I. B. K. C. Gupta Ramesh Garg and P. Bhartia, *Microstrip Lines and Slotlines*, 2nd. Artech House Boston, London, 1996.
- [89] I. Bahl, *Lumped Elements for RF and Microwave Circuits*, 1st. Artech House, Boston, London, 2003.
- [90] P. P. Labs. (), [Online]. Available: http://www.picosecond.com/product/category.asp?pd_id=10.
- [91] J. C. M. H. Renfeng Jin Subrata Halder and C. L. Law, "Sub-nanosecond greater-than-10v compact pulse amplifier with improved linearity and reduced power consumption," *IEEE International Symposium on Radio-Frequency Integration Technology*, 2009.